

Jovian Dynamics. Part III: Multiple, Migrating, and Equatorial Jets

G. P. WILLIAMS

NOAA/Geophysical Fluid Dynamics Laboratory, Princeton University, Princeton, New Jersey

(Manuscript received 2 October 2001, in final form 12 December 2002)

ABSTRACT

Studies of the dynamical response of thin atmospheric layers overlying thick envelopes are extended to examine how multiple jets, such as those seen on Jupiter and Saturn, can be generated and maintained. The jets are produced by baroclinic instabilities and are examined numerically using a primitive equation model subject to simple heating functions. The motions are confined to a thin upper layer by a heating that produces a flow with either an exponential vertical structure or one that is linear aloft while vanishing below. The motions are driven by latitudinal heating distributions with a variety of global and local components.

The calculations show that jets roughly resembling the main Jovian ones in amplitude, scale, and form can be generated and maintained in a steady configuration when the flow has the confined linear structure. When the flow has the exponential structure, however, the jets migrate slowly but continuously equatorward while being regenerated in higher latitudes. For both structures, the flow is sensitive to the heating distribution in low latitudes where jets form only if a significant baroclinicity exists in that region; such jets can also be barotropically unstable and can generate a superrotating current at the equator. In midlatitudes, except for being confined to an upper layer, the baroclinic instabilities resemble the standard forms seen in terrestrial models with high rotation rates.

Additional calculations show that superrotating equatorial currents can also be generated for deep layers or for Earth's atmosphere if the initial instabilities are developed in low latitudes. Broad easterly currents such as Neptune's can also be generated by elementary heating distributions, provided that the heated layer becomes progressively thicker with latitude. Finally, the hexagonal shape that high-latitude jets sometimes assume on Saturn when viewed in a polar projection can be attributed to nonlinear waves associated with baroclinic instabilities.

1. Introduction

We continue the presentation begun in Williams (1996, hereafter Part I) and extended in Williams (2002, hereafter Part II) of solutions to a primitive equation model that examine dynamical processes thought to be relevant to the global circulations of the Jovian atmospheres. Here, the main concern is with generating the multiple jet streams and an equatorial superrotation of the form and scale seen on Jupiter and Saturn. In addressing this problem, we again explore the hypothesis that the active atmosphere is driven by baroclinicity and is thin relative to a deep underlying envelope. The vertical structures confining the motions to the upper layer are assumed to be of the same form as those known to favor the existence of stable planetary vortices.

In Part I, thin jets were seen to be capable of generating and coexisting with thin planetary-scale vortices that are absolutely stable when all of the horizontal motions are limited to the upper layer by exponential stratifications with a high confinement rate. Such stratifi-

cations, denoted by EXP, have a related structure, denoted by LIN, whose horizontal flow and Brunt-Väisälä stability are linear in the thin upper layer but zero below; see Fig. 1. The LIN structure allows a similar vortex behavior but has different small-scale baroclinic instability properties, particularly as regards the latitudinal eddy heat and momentum fluxes. These similarities and differences are examined in this paper for issues relating to the genesis and equilibration of jets.

In Part II, the extension of vortex modeling to a wider range of latitudes indicates that the EXP and LIN structures could occur globally. The vortices are generated in anticyclonic zones by the long-wave baroclinic instability of baroclinic easterly jets and their relation to the long-wave solitary Rossby waves provides, via the propagation rate, a deformation radius of about 1000 km as an upper limit for the size of the eddies that sustain the jets. In addition, the creation of steady vortex configurations using a Newtonian heating function provides an estimate of about 300 days as a representative timescale for the thermal processes. These space scales and timescales are also used in this study.

The latitudinal distribution of Jupiter's zonal winds is well known at cloud level due to the high accuracy

Corresponding author address: Dr. G. P. Williams, NOAA/GFDL, Princeton University, P.O. Box 308, Princeton, NJ 08542-0308.
E-mail: gw@gfdl.noaa.gov

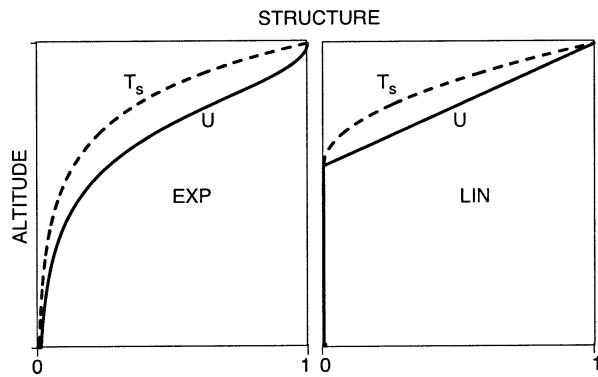


FIG. 1. Schematic diagram of the static stability and the vertical form of the zonal flow produced by the LIN and EXP heating systems, shown for the upper regions only.

that the cloud tracking method allows; see Simon (1999) for a recent synthesis. Both hemispheres contain about six westerly jet streams, separated by weaker easterly flows, between the equator and $\pm 60^\circ$ latitude. Starting from a superrotation of about 100 m s^{-1} at the equator, the zonal flow increases into the Tropics to peak at $\pm 8^\circ$ latitude with a particularly intense maximum of 170 m s^{-1} occurring in the Southern Hemisphere. The winds then drop off rapidly with latitude and alternate from easterly to westerly with steadily decreasing amplitudes and inferior easterly components.

Little is known directly about the vertical wind structure on Jupiter apart from the measurement made by the *Galileo* entry probe at 6.5°N latitude, which revealed a zonal flow that remains uniform at 170 m s^{-1} over the 100-km layer between 4 and 21 bars, at least for the longitudinal range and time span sampled (Atkinson et al. 1998). This amplitude closely matches the value of the angular momentum conserving wind, $u_m = a\Omega \sin\phi \tan\phi$, at this latitude (Williams 1997) and its compliance with a standard meteorological measure suggests that the motions could be shallow in the vertical. However, the nature of the winds measured by the *Galileo* probe has undergone reassessment (Young 1998; Allison 2000) following the realization that the spacecraft entered an anomalous warm vortex. As regards the related thermal structure, the *Galileo* probe revealed a statically stable troposphere (Seiff et al. 1998, Fig. 36) with complex variations similar to those predicted by vortex theory (Part I, Figs. 40 and 45).

The existence of multiple jets is usually explained theoretically in terms of the barotropic and baroclinic modes of energy and enstrophy cascade associated with the various forms of β turbulence, as described by Rhines (1975, 1977, 1994). Consequently, the generation and persistence of multiple jets have been explored numerically using a variety of atmospheric, oceanic, and planetary models. The models range from barotropic spheres (Williams 1978; Huang and Robinson 1998; Huang et al. 2001), to quasigeostrophic (QG) beta planes (Williams 1979; Panetta 1993; Vallis and Maltrud

1993; Treguier and Panetta 1994; Lee 1997), to shallow water spheres (Williams and Wilson 1988; Cho and Polvani 1996), to primitive equation general circulation models (GCMs) (Williams 1988).

The generation of multiple jets in thin baroclinic layers has not been evaluated until now, and it is not obvious that the baroclinic instability needed to energize the small eddies and the cascades needed to drive the jets can occur in such systems. In fact, linear QG theory for baroclinic ocean layers implies the opposite (Gill et al. 1974), that westerly currents are usually stable in exponential structures. Neither is the extent known to which baroclinic instability can be extended into low latitudes. Such processes could be responsible for, or at least influence, the onset of an equatorial superrotation. Other hypotheses, in various stages of development, have been suggested for the possible cause of the multiple jets; their processes range from deep convection (Busse 1994; Condie and Rhines 1994), to shallow convection (Williams and Robinson 1973; Williams 1978), to moist convection (Gierasch 1976; Ingersoll et al. 2000), and on to thin baroclinic layers overlying deep barotropic flows (Orsolini and Leovy 1993). Here, we chose to evaluate the simplest hypothesis first.

To examine the hypothesis that baroclinic instabilities can generate and maintain multiple jets in a thin atmosphere at all latitudes, calculations are made with a primitive equation model subject to a Newtonian heating function. The heating produces flows with either the LIN or EXP vertical structure and thence two forms of baroclinic instability and two classes of jet. The latitudinal heating distribution is set experimentally to develop a variety of global and local baroclinicities that examine the sensitivity of the circulation to the heating imbalance, especially in low latitudes.

The presentation begins in section 2 with a description of the basic model, the parameters, and the formulation of the heating distributions. This is followed by a brief review of those theories that help in designing the calculations and in understanding the solutions. Section 3 then gives an overview of those solutions that describe the range of jets found for the various heating arrangements, particularly those needed to isolate the conditions for the onset of equatorial westerlies in both structures. The LIN and EXP systems produce two distinct classes of circulation, the first giving steady flows and the latter producing jets that migrate equatorward and regenerate in high latitudes. Section 4 proceeds to examine in detail the two LIN solutions that exhibit the most basic and the most realistic circulations.

Likewise, section 5 concentrates on details of the most basic and the most realistic EXP solutions to examine the nature of baroclinic instabilities in a system that allows jets to migrate. To define processes more clearly, we then limit the domain to low latitudes in section 6 and examine the behavior of a solitary tropical jet. This also leads to a derivation of the conditions under which instabilities can produce equatorial west-

TABLE 1. Basic heating parameters for the functions defined in section 2c and Fig. 2, for the jet-genesis cases with the LIN vertical structure. The L6 case has a longer 180° domain, plus a Gaussian cooling dip, written as $g(-10^\circ, 4^\circ, -0.25)$ to denote, its latitudinal center, half-width, and amplitude relative to unity.

Case	Rates		Latitudes $P(\phi_i)$	Amplitudes $P(a_i)$	Form $P(\phi)$
	ΔT	δT			
L1	6	4	$-(0, 70)^\circ$	(1, 0)	P_2
L2	6	4	$-(0, 10, 70)^\circ$	(1, 1, 0)	BT + BC
L3	8	4	$-(0, 2, 70)^\circ$	(1, 1, 0)	BC
L4	6.5	4	$-(0, 6, 12, 70)^\circ$	(1, 1, 0.8, 0)	BT + 2BC
L5	7	4	$-(0, 10, 70)^\circ$	(1, 0.75, 0)	2BC
L6	6	4	$-(0, 10, 70)^\circ$	(1, 1, 0)	BT + BC + DIP

erlies in Earth's atmosphere. Then, to test the relevance of the thin-layer hypothesis even further, section 7 turns to some anomalous cases to show first how a major easterly current can be produced in mid- to low latitudes, as on Neptune, and then how hexagonal jets can occur in mid- to high latitudes, as on Saturn. The planetary implications of the main solutions are touched upon when concluding in section 8.

Finally, note that some of the new processes described by the solutions, particularly those in low latitudes, have also been reproduced in global atmospheric models, including a multilevel, spectral, pressure-coordinate GCM for Earth; the results for the latter are discussed in a separate paper (Williams 2003a). The variability of the jets as the extent of the baroclinic layer goes from shallow to deep is also discussed elsewhere (Williams 2003b).

2. Model and theory

a. System of equations

The numerical studies use the primitive equations of motion with a Boussinesq equation of state, solved for a regional channel on a sphere. This model provides an adequate representation of the basic dynamical mechanisms under consideration and can be applied to either an ocean or an atmosphere provided that, for the latter, the variables are mapped from geopotential to pressure coordinates and reinterpreted appropriately, as described, for example, by Salmon (1998, p. 102).¹ The primitive equation model for a thin hydrostatic fluid is specified by the zonal, meridional, and vertical velocity components u , v , w , and by the pressure, density, and temperature fields p , ρ , T . The standard equations are written in spherical coordinates, as in (1)–(14) of Part I, and include simple biharmonic and Laplacian diffusion terms with coefficients ν_4 and ν_2 in the horizontal and vertical, respectively, as well as a heating function and a convective adjustment. The variables λ , ϕ , z represent the longitude, latitude, and height; g is gravity; Ω and a are the planetary angular velocity and radius;

$f = 2\Omega \sin\phi$ and $\beta = 2\Omega a^{-1} \cos\phi$ are the Coriolis parameters; T_s and α are the background hydrostatic temperature and the Boussinesq coefficient; while $B = \alpha g T_s^*$ and $T^* = T + T_s$ define the Brunt–Väisälä stability parameter and the total temperature.

The equations are solved using the finite difference methods documented in Part I; these involve a leapfrog time differencing and a centered spatial differencing on the so-called B grid. The computational domain consists of a Southern Hemisphere channel with periodic boundary conditions in longitude, symmetry conditions at the northern boundary on the equator, together with a no-slip, no-flux condition on the southern wall. In the vertical, both surfaces are taken to be horizontal rigid lids with free-slip, no-flux conditions at $z = 0$ and $-H$, where H is the fluid thickness. Near the lower surface, a weak linear drag with a timescale τ_D helps equilibrate some flows.

b. Parameter values

The calculations use parameter values that are thought to be appropriate for Jupiter's atmosphere, values that produce zonal jets with amplitudes, scales, and form comparable to those observed at cloud level. The planetary parameters, $a = 71\,300$ km, $\Omega = 1.76 \times 10^{-4}$ s⁻¹, and $g = 26$ m s⁻², remain fixed while the following represent the basic values about which variations are made in Tables 1–3. For evaluation purposes, H is nominally set at 15 000 km but, as discussed in Part II, it can be reduced by a factor of 10 or more and all solutions can be rescaled in the vertical without altering their form, provided that the temperature gradients are increased (within the observational limits) by a corresponding factor to maintain identical winds. The Boussinesq coefficient is kept fixed at $\alpha = 0.005^\circ\text{C}^{-1}$, an arbitrary value, and the diffusion coefficients are set close to $\nu_4 = -10^{17}$ m⁴ s⁻¹ and $\nu_2 = 0$.

The domains generally range over 60° longitude and 70° latitude, with $\Delta\lambda = 1^\circ$ and $\Delta\phi = 1^\circ$ forming the standard grid spacing, and with $\Delta t = (1/100)$ day being a typical time step.² For the EXP cases whose structure goes as $\exp(Nz')$, the vertical grid Δz also varies ex-

¹ The model fails, however, to represent the dynamics of the upper atmosphere or the deepest layers but these lie beyond the intended scope of this study.

² A day equals 86 400 s in this paper.

TABLE 2. Basic heating parameters for the functions defined in section 2c and Fig. 2, for the jet-genesis cases with the EXP vertical structure. The vertical confinement rate N equals 200 in all cases. The E5 and E6 cases have a Gaussian cooling dip, written as $g(-12^\circ, 4^\circ, -0.1)$ to denote its latitudinal center, half-width, and amplitude relative to unity.

Case	Rates		Latitudes $P(\phi_i)$	Amplitudes $P(a_i)$	Form $P(\phi)$
	ΔT	δT			
E1	30	4	$-(0, 70)^\circ$	(1, 0)	P_2
E2	25	4	$-(0, 12, 70)^\circ$	(1, 1, 0)	BT + BC
E3	25	4	$-(0, 6, 70)^\circ$	(1, 1, 0)	BT + BC
E4	25	4	$-(0, 2, 70)^\circ$	(1, 1, 0)	BC
E5	20	4	$-(0, 12, 70)^\circ$	(1, 1, 0)	BT + BC + DIP
E6	25	4	$-(0, 12, 70)^\circ$	(1, 1, 0)	BT + BC + DIP

ponentially in its spacing, usually as $\exp(7z')$ when the confinement rate N equals 200, to put more than half the grid points in the active layer, where $z' = z/H$. In the LIN cases, a simple split grid with $\Delta z = [\Delta z_1, \Delta z_2] = [0.05, 0.95]2H/KZ$, puts one-half of the grid points, the thinly spaced ones, in an upper layer of thickness $h_1 = H/20$ that more than contains the main motion, and the other half, the thickly spaced ones, in the abyss; the number of grid points KZ usually equals 20.

For the two Earth cases discussed in section 6b, the basic parameters are $a = 6400$ km, $\Omega = 7.3 \times 10^{-5}$ s $^{-1}$, $g = 9.8$ m s $^{-2}$, $H = 8$ km, $\alpha = 0.003^\circ\text{C}^{-1}$, $\nu_4 = -10^{15}$ m 4 s $^{-1}$, $\nu_2 = 0$; for a domain resolved by grids with $\Delta\lambda = 3^\circ$, $\Delta\phi = 1^\circ$, $\Delta z = H/20$, and $\Delta t = (1/100)$ day.

In presenting the solutions, the figures use solid contour lines to plot values greater than or equal to zero, while dashed lines denote negative values. For the time-mean eddy transports, evaluated using fields sampled at 1-day intervals, the zero-value contours are omitted from the plots for greater clarity. The temperature plots exclude the background component except when referred to as the total temperature. Altitude is measured in kilometers in the vertical cross sections. Indices are used to refer to phenomena by zone, starting at the equator, so that W_0 refers to the superrotating westerly, followed by W_1 and E_1 for the low-latitude westerly and easterly, and thereafter by W_i and E_i ($i = 2, 3, \dots$) for the numerous midlatitude currents.

c. Heating functions

All flows are developed from rest and maintained by a Newtonian heating function of the form

$$\frac{\partial T}{\partial t} \dots = \frac{T_r - \bar{T}}{\bar{\tau}} - \frac{T'}{\tau'}, \quad (1)$$

where the heating rate is proportional to the difference between the fluid temperature and a specified radiative–convective equilibrium temperature $T_r(\phi, z)$. The radiative–convective damping time $\tau(\phi, z)$ is set to constant values but, for computational expediency, uses the split form with $\bar{\tau} \ll \tau'$ to maintain the zonal mean (bar) fields without significantly dampening the eddy (prime) fields. This distinction has little effect. Following Part

II, the axisymmetric state is usually spun up with $\bar{\tau} = 10$ days for 100 days, then perturbed and the resulting flow maintained with $\bar{\tau} = \tau_D = 300$ days and $\tau' = 1000$ days.

The following nonseparable form is used to heat the confined layer:

$$T_r = \Delta T P(\phi) S(z) + T_s(z), \quad (2)$$

where in the EXP system the structure has the refined form $S = (d/dz)[\text{sech}(Nz')]$ to produce $u(z)$ profiles that are exponential at depth while having a vanishing shear over the upper atmosphere (see Fig. 1) in line with the *Galileo* data (Williams 1997). The hydrostatic temperature, $T_s(z) = \delta T \exp(Nz')$, is independent of latitude. The amplitudes ΔT and δT set the baroclinicity and hydrostatic stability rates. For the LIN system, the structures are defined, as in Part I, by the split functions $S = C[1, 0]$ and $T_s = \delta T C[z_c^2, 0]$, where C symbolizes confinement and where the first factor defines the distribution in an upper region of depth $h \approx 0.7h_1$, with $z_c = 1 - |z/h|$ over $|z| \leq h$. The second factor defines the abyssal distribution. The upper region extends over about seven grid points when $KZ = 20$, so the main motions always lie well within the highly resolved layer and experience no computational problems at the Δz_1 to Δz_2 interface.³ The ratio $\delta = h/H$ defines the confinement parameter for the LIN system.

To provide a global baroclinicity, the latitudinal heating distribution $P(\phi)$ is first based on the second Legendre polynomial and set equal to $\cos^2\phi$ —denoted as $P_2(\phi)$ in form 1 of Fig. 2—where only positive values are used so as to avoid cooling and inducing large-scale convection in the confined layer. As the P_2 distribution is not universal enough to yield the full range of circulations, the form of $P(\phi)$ is varied and evolved toward greater complexity by introducing separate barotropic and baroclinic zones. We begin by examining the influence of a barotropic (BT) zone at the equator by varying its extent into the Tropics, in effect replacing P_2 by

³ This was verified by comparison with calculations using uniform or exponential grids.

TABLE 3. Basic heating parameters for the functions defined in section 2c and Fig. 2, for the cases relating to (i) the equatorial superrotation on Jupiter in Q1 and on Earth in Q2 and Q3; (ii) planets with atmospheres of variable depth in P1 and P2; and (iii) planets with hexagonal flows in P3. The P3 case has a Gaussian cooling dip, written as $g(-9^\circ, 5^\circ, -0.25)$ to denote its latitudinal center, half-width, and amplitude relative to unity. Earth cases have $\tau = 20$ days, $\tau_D = 1$ day, a thick LIN2 structure with $S(z) = 1$ and $T_s(z) = \delta T z'$, and diffusion coefficients $\nu_4 = -10^{15} \text{ m}^4 \text{ s}^{-1}$, with $\nu_2 = 0$ for Q2 and $\nu_2 = 0.2 \text{ m}^2 \text{ s}^{-1}$ for Q3. (a) For Q2 the heating profile is normalized over 70° of latitude. Cases P1 and P2 have the special $N(\phi)$ structure defined in (10).

Case	Rates		Latitudes $P(\phi_i)$	Amplitudes $P(a_i)$	Form $P(\phi)$	Structure $S(z)$
	ΔT	δT				
Q1	2.2	4	$-(0, 15, 40)^\circ$	(1, 1, 0, 0)	BC LL	LIN
Q2	30	40	$-(0, 70)^\circ$	1	$\cos^2 \phi^{(a)}$	LIN2
Q3	30	40	$-(0, 70)^\circ$	1	$\cos^8 \phi$	LIN2
P1	30	5	$-(0, 80)^\circ$	(1, 0)	P_2	$N(\phi)$
P2	25	5	$-(0, 80)^\circ$	(1, 0)	P_2	$N(\phi)$
P3	6	4	$-(0, 9, 70)^\circ$	(1, 1, 0)	BT + BC + DIP	LIN

$P_{\text{BT+BC}}$, a combination of a tropical BT zone and a mid-latitude baroclinic (BC) zone⁴—form 2 in Fig. 2.

We are particularly interested in determining what factors control the location, especially the lowest latitude, at which jets can be generated and what heating forms are needed to develop an equatorial superrotation. To begin addressing such issues, a simple P_{BC} heating—form 3 in Fig. 2—is used to extend the baroclinicity to

⁴ By *barotropic* or *baroclinic* zones, we mean regions with latitudinally uniform or latitudinally linear heating distributions, respectively.

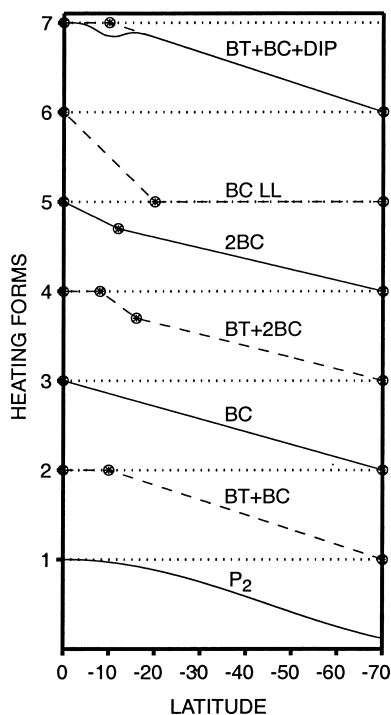


FIG. 2. Schematic diagram showing the progression of the latitudinal heating distribution used in the calculations. The profiles are referred to in the text as the P_2 , $P_{\text{BT+BC}}$, P_{BC} , $P_{\text{BT+2BC}}$, $P_{2\text{BC}}$, P_{BCLL} , and P_{DIP} forms, where BT, BC, LL, and DIP indicate barotropic, baroclinic, low-latitude, and Gaussian components, respectively.

the equator to gauge its effect upon the tropical flow. Then, to encourage jets to form more readily in low latitudes, a stronger baroclinicity is introduced there, together with the normal barotropic and baroclinic zones elsewhere, to give a $P_{\text{BT+2BC}}$ distribution—form 4 in Fig. 2. Form 5 does the same but excludes the barotropic zone, as does form 6, which is reserved for developing solitary low-latitude jets.

The evolution of $P(\phi)$ ends with a P_{DIP} distribution—form 7 in Fig. 2—which is equivalent to form 2 with a Gaussian cooling component added to boost the baroclinicity in low latitudes, making it similar in effect to form 4 or 5 but allowing a different way of creating and interpreting the distribution. Heating profiles resembling P_{DIP} have been used in dry Earth models to allow implicitly for the intense heating gradient produced by condensation at the equator (Smagorinsky 1963, Fig. A5). All of the $P(\phi)$ profiles in Fig. 2 are smoothed and normalized to vary between 0 and 1; the tables document the variety of amplitudes a_i and latitudes ϕ_i associated with each zone, starting at the equator. In retrospect, a more systematic approach would involve setting $P(\phi) = c_2 \cos^2(\phi) + c_n \cos^n(\phi)$, where c_2 and c_n are constants for $n = 4, 8, \text{ or } 16$, as in Williams (2003a).

d. Theoretical background

For thin layers, as for thick,⁵ linear baroclinic instability theory can be used to explain eddy origin and scale, and nonlinear theory can be used to explain eddy evolution and fluxes. In the classic ocean study of Gill et al. (1974) for exponentially structured flows, the latitudinally independent, quasigeostrophic flows on a beta plane can be unstable if the potential vorticity gradient

$$q_y = \beta + f \left(\frac{\rho_y}{\rho_z} \right)_z = \beta - \left(\frac{u_z}{s} \right)_z \quad (3)$$

changes sign internally or opposes the sign of u_z at the upper boundary, where $s = B/f^2$ and y is the meridional

⁵ By *thin* or *thick* layers, we mean layers for which the motion is either confined aloft or extends over the entire fluid.

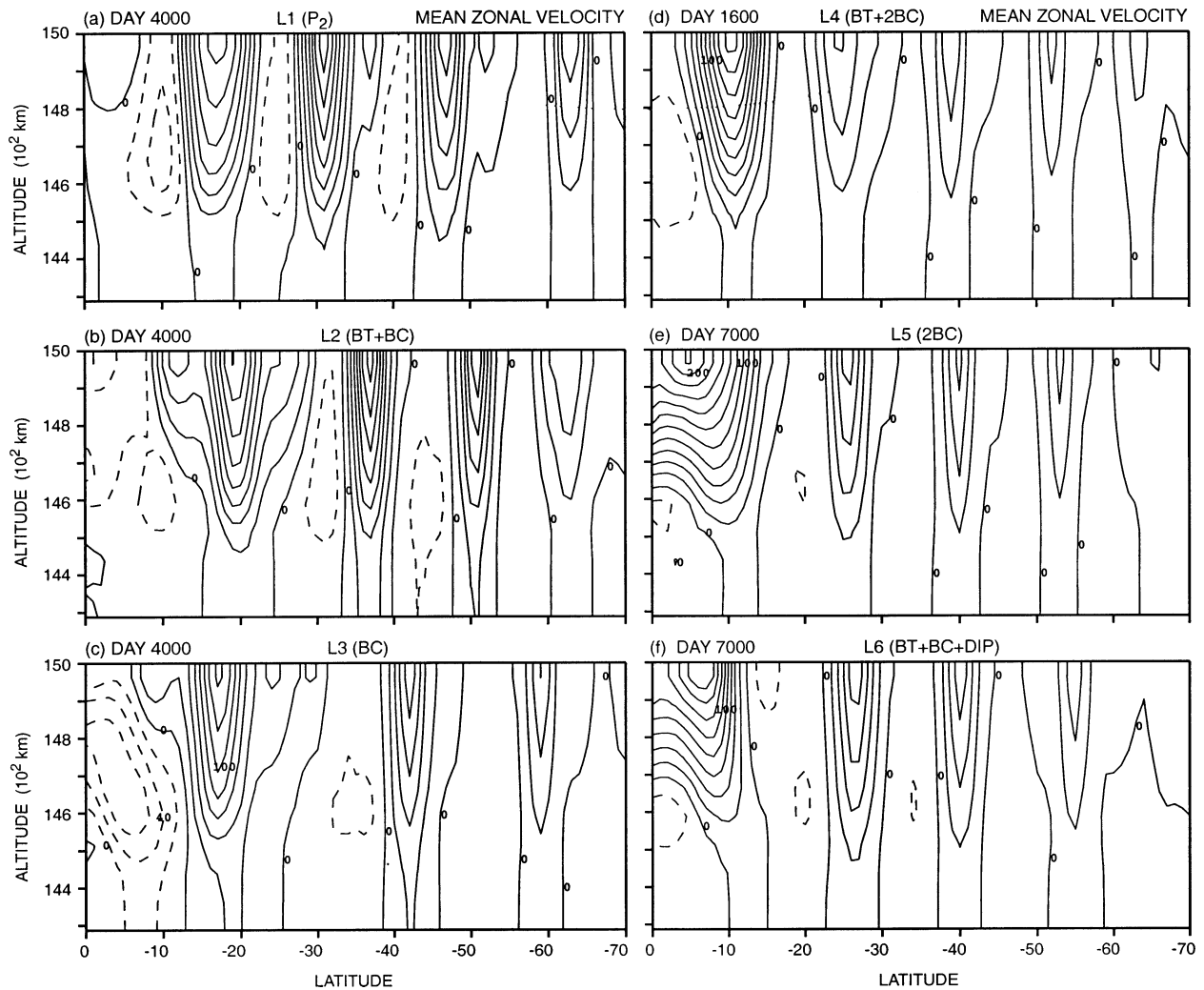


FIG. 3. Meridional sections of the mean zonal velocity $\bar{u}(\phi, z)$ for the six cases L1–L6, with LIN vertical structures for the various forms of $P(\phi)$ heating distribution, shown at the end of each calculation. Labels denote the number of barotropic (BT), baroclinic (BC), and Gaussian (DIP) components in each latitudinal heating distribution. The contour interval equals 10 m s^{-1} for L1–L2, and 20 m s^{-1} for L3–L6, with maxima equal (78, 80, 145, 186, 220, 178) m s^{-1} and minima equal $(-25, 31, 79, 39, 25, 36) \text{ m s}^{-1}$ in L1–L6, respectively.

coordinate. Instability is primarily determined by the slope of the isopycnals. When the slope is uniform, only easterly flows are unstable. To destabilize the westerly flow produced by the standard atmospheric heating requires that the symmetry between the $u(z)$ and $B(z)$ distributions in exponential systems be broken.

The necessary asymmetry can be achieved by modifying either the shear or the stability, by one of the simple combinations

$$u(z) = u_0 e^{z/d} - u_1 e^{z/b}, \quad s(z) = s_0 e^{z/d}, \quad (4)$$

$$s(z) = s_0 e^{z/d} + s_1 e^{z/b}, \quad u(z) = u_0 e^{z/d}, \quad (5)$$

provided that $d < b$, where d and b are depth parameters. The first combination, as Gill et al. (1974) show, can have a maximum zonal flow below the upper surface where it produces a weak instability. Both forms of asymmetry occur in the numerical solutions where the

static stabilities have a strong jet-related component B_j that tends to dominate the background component B_s aloft.

For the larger planetary scales of interest here, the results given by the advective model of baroclinic instability, as derived by Fjortoft (1951) and evaluated for arbitrary $u(z)$ profiles by Spar (1957) and Wiin-Nielsen (1967), apply to both the LIN and EXP structures. The vertical heat transport term Bw is assumed to be negligible in this model, which makes it useful for understanding flows that may have a non-QG balance or may have a complex or negligible $B(z)$. The analysis of Wiin-Nielsen (1967) for arbitrary $u(z)$ profiles shows that disturbances of the form $\exp[ik(x - ct)]$ have a phase speed given by

$$c = \left(I_1 - \frac{c_r}{2} \right) \pm \left(I_1^2 - I_2 + \frac{c_r^2}{4} \right)^{1/2}, \quad (6)$$

where $c_r = \beta/k^2$, $I_1 = \int_0^1 u dz'$, $I_2 = \int_0^1 u^2 dz'$. Instability occurs according to Schwartz's inequality when $I_2 - I_1^2 > c_r^2/4$, which implies that westerlies are unstable at scales $L < L_\beta(2/N)^{1/4}$ and $L < L_\beta(2h/H)^{1/2}$ in the EXP and LIN systems, respectively, where $L_\beta = (U/\beta)^{1/2}$ for the velocity scale U . For the numerical cases with $N \sim 200$ or $\delta \sim 1/20$, the cutoff occurs at $L \sim L_\beta/4$. This upper limit to the scale of the baroclinic instability implies that a horizontal grid of approximately 1000 km is needed in the calculations. Similar criteria for the instability of thin-layer westerlies are given by Killworth (1980, section 9b) and Benilov (1995, section 5).

The nonlinear baroclinic instability theories that follow eddy development through cycles of growth and decay, and help explain eddy evolution and fluxes in Earth's atmosphere, appear to be relevant to thin layers also. Detailed analyses of such "eddy cycles" indicate that, for a specified zonal flow, linear theory applies initially, with the eddy energy growing at all heights but transporting heat mainly at lower levels (Simmons and Hoskins 1978; Edmon et al. 1980). The upper-level eddies, fed by upward wave radiation, generate planetary waves that propagate to other latitudes. These waves produce a large momentum flux that either traverses poleward, as in the standard terrestrial case, or converges on the jet cores, as in terrestrial models with higher rotation rates (Williams 1988).

Quasigeostrophic turbulence theory analyzes more general forms of energy and enstrophy cascade and gives insight into processes that determine the jet scale. According to this theory (Rhines 1975, 1977), the Coriolis gradient β stops the nonlinear barotropic cascade at a wavenumber $\hat{k}_\beta = (\beta/\hat{U})^{1/2}$ that separates the wave and turbulence regimes and thereby defines the Rhines jet scale as $\hat{L}_R = \pi(\hat{U}/\beta)^{1/2}$, where \hat{U} is the root-mean-square barotropic eddy velocity. For baroclinically unstable flows, this barotropic velocity can be related to the baroclinic eddy velocity \hat{U} by using scaling arguments to connect the barotropic energy level to the rate of eddy energy production, Held and Larichev (1996). This leads to a "baroclinic" version of the Rhines wavenumber, $\hat{k}_\beta = \beta\Lambda/\hat{U}$, where $\Lambda = hB^{1/2}/f$ is the deformation radius. This analysis can be further extended to thin layers (Smith and Vallis 2002) to give an alternative scale for the jet widths, $\hat{L}_R = \pi(2\delta)^{1/2}(\hat{U}/\beta\Lambda)$. Although the processes involved in the solutions differ from those invoked in the theoretical derivation, this length scale seems to apply to the numerical and Jovian jets and seems to be preferable for flows with a small or uncertain barotropic component, with $\hat{U} \ll \hat{U}$. In particular, the typical modeling scales $\hat{U} = 50 \text{ m s}^{-1}$, $\delta = 1/30$, $\beta = 0.4 \times 10^{-8} \text{ km}^{-1} \text{ s}^{-1}$, and $\Lambda = 10^3 \text{ km}$ yield a reasonable value, $\hat{L}_R = 10\,000 \text{ km}$, comparable to Jupiter's jet widths. The \hat{L}_R scale also resembles the optimal eddy size, $L_c = 2\pi h U_z / \beta \Lambda$, predicted by Charney's linear instability analysis (Gill 1982, section 13.4). In practice, the various scales are too close to each other

in value to determine which processes are involved in defining the jet scales.

3. The range of multiple jets

We begin our discussion of the numerical solutions by giving an overview of the circulation range as defined by the mean zonal flows in Figs. 3 and 4. The flows are generated by the various heating distributions described in section 2c using the parameters listed in Tables 1 and 2. The heating profile evolves from the elementary P_2 form to the complex P_{DIP} profile so that the baroclinicity can be extended into lower latitudes to produce a tropical W_1 jet whose barotropic instability generates a W_0 superrotating current at the equator. Two classes of circulation are obtained as the LIN and EXP structures support significantly different flows, with the latter exhibiting novel equatorward-migrating jets. The dynamics of the main cases are discussed in detail later in sections 4 and 5.

a. The LIN jet range

The representative set of solutions for the LIN structure, L1–L6 in Fig. 3, shows how the circulation progresses as the level of complexity in the $P(\phi)$ heating profile increases. The simplest circulation occurs for the elementary $P_2(\phi)$ heating form and consists of four westerly jets, W_{1-4} , over the 70° domain (Fig. 3a). Weak easterly currents form near the equator and between the westerly jets. The lowest latitude at which a jet core lies is 17°S , where the stable W_1 current is essentially a residual of the axisymmetric thermal wind that is truncated on its poleward side by the action of the eddies associated with the midlatitude jets.

To examine the sensitivity of the W_1 jet to the way the heating distribution allocates the barotropic and baroclinic zones, the P_2 variation is first replaced by a two-component function that has a purely barotropic part from the equator to 10°S and a linear baroclinic part over the rest of the domain, as in form 2 of Fig. 2. The main effect of this $P_{\text{BT+BC}}$ heating for the L2 case in Fig. 3b is to produce a wider W_1 jet with a more poleward core at 20°S than in the L1 case. The L1–L2 similarity raises questions about the dependence of the W_1 jet and the E_0 current that lies equatorward of it, on the width of the tropical barotropic zone and on the existence of baroclinicity in low latitudes. To address these issues in the L3 case, the baroclinicity is extended to within 2° of the equator, as in the P_{BC} profile of Fig. 2. The resulting flow in Fig. 3c resembles the L1 and L2 forms, though the jets are fewer because they are stronger. The tropical baroclinicity does not shift the W_1 jet equatorward because wave propagation produces a strong E_0 easterly current near the equator.

To really move the W_1 jet toward the equator, without altering the midlatitude jets, requires the introduction of a stronger and separate baroclinicity in lower lati-

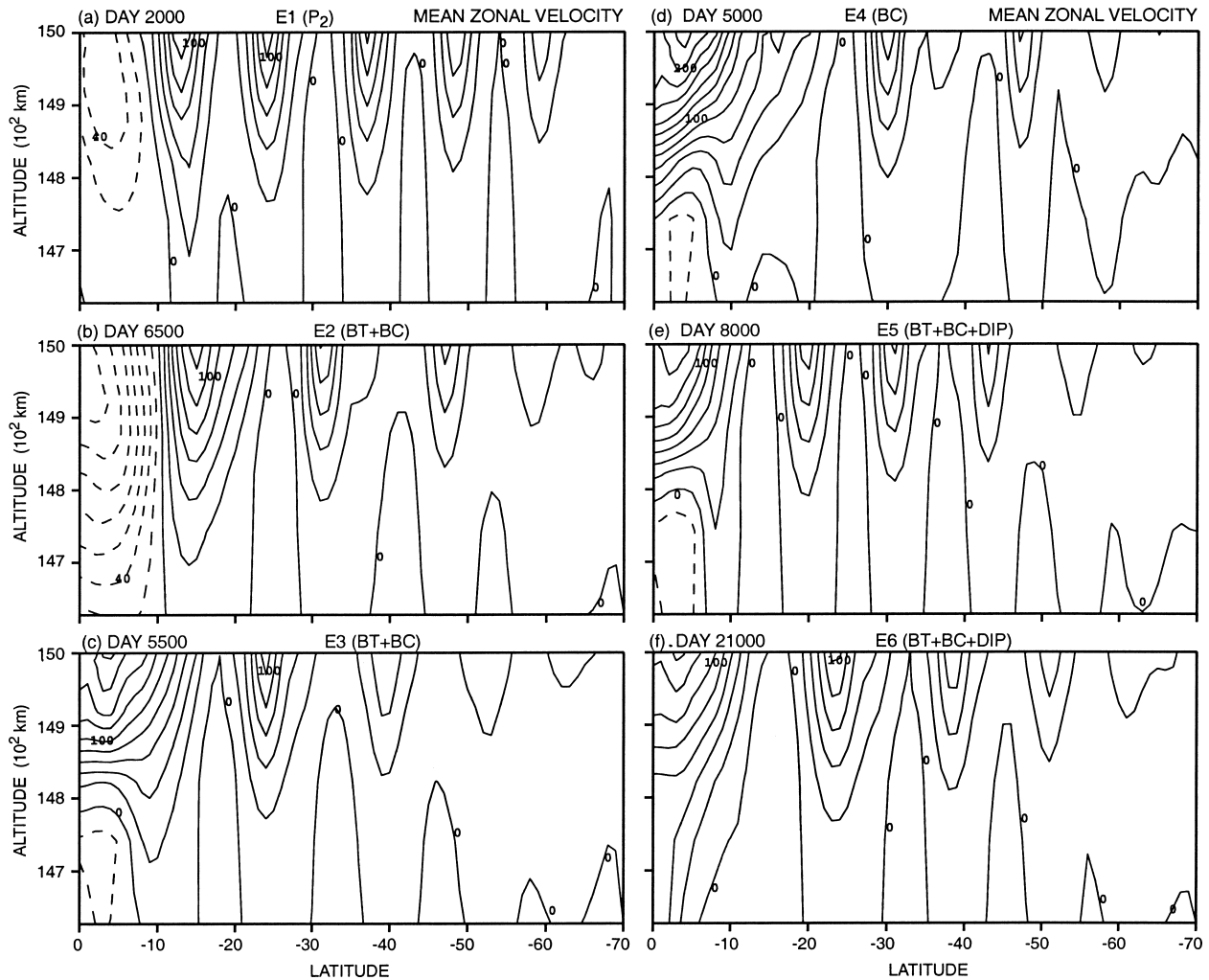


FIG. 4. Meridional sections of the mean zonal velocity $\bar{u}(\phi, z)$ for the six cases E1–E6, with EXP vertical structures for the various forms of $P(\phi)$ heating distribution, shown at the end of each calculation. Labels as in Fig. 3. The contour interval equals 20 m s^{-1} in all cases, with maxima equal (113, 131, 186, 232, 158, 144) m s^{-1} and minima equal $(-57, 153, 28, 26, 36, 14) \text{ m s}^{-1}$ in E1–E6, respectively.

tudes, as in form 4 of Fig. 2. For such a $P_{\text{BT}+2\text{BC}}$ heating in the L4 case, the barotropic zone goes from the equator to 6°S while the stronger baroclinic zone extends from 6° to 12°S (Table 1). The latter produces a strong W_1 jet centered at 10°S , clearly a significant equatorward shift and one that leads to a five-jet circulation in the domain as a whole (Fig. 3d). Although there is much eddy activity in low latitudes, it does not lead to the onset of a W_0 current at the equator. This result, however, is conditional and depends on the width of the barotropic zone. When the barotropic zone extends from the equator to a critical latitude that lies somewhere between 3° and 6°S , other calculations reveal that the W_1 jet then lies sufficiently near the equator for its instability to generate a W_0 current. For the parameter range under consideration, the W_1 jet must be centered at $|\phi| \leq 8^\circ$ and must be sufficiently strong for this to happen.

In the limiting L5 case, a stronger baroclinicity ex-

tends all the way to the equator from 10°S in the $P_{2\text{BC}}$ heating and produces a W_1 jet at 8°S whose strong instability generates eddies capable of driving a strong W_0 superrotation at the equator (Fig. 3e). Another way of increasing the tropical baroclinicity is by introducing a local Gaussian cooling dip at the intersection between the barotropic and baroclinic zones, at 10°S in form 7 of Fig. 2. In the L6 case, such a P_{DIP} heating produces an unstable W_1 jet at 8°S and a W_0 superrotation at the equator (Fig. 3f). As noted in section 2c, the stronger baroclinicity needed to produce an equatorial westerly can be represented by either a $P_{2\text{BC}}$ or a P_{DIP} heating distribution, which in turn can be ambiguously interpreted as being due either to a powerful latent heating at the equator or to albedo variations in a cloudy atmosphere.

All of the LIN jets are steady once the flow has fully evolved and are fully represented by the typical $\bar{u}(\phi, t)$ diagram for the L6 case in Fig. 5a. Most of the jets

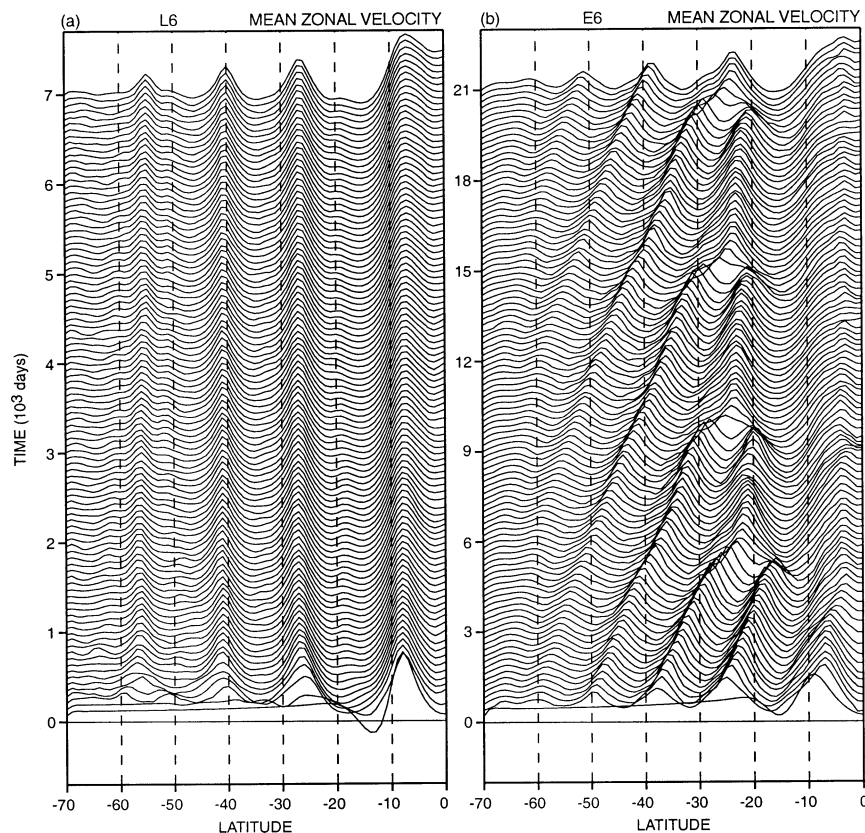


FIG. 5. Time sections of the mean zonal velocity for the L6 and E6 cases, sampled near the top surface. Scales for the maximum \bar{u} are (a) 147 and (b) 150 m s^{-1} , and both are equivalent to 10 times the vertical spacing between the curves.

equilibrate completely within the first 1000 days but the equatorial W_0 current, when it occurs, grows more slowly and takes about 5000 days to equilibrate, which it does by modifying the W_1 instability. Figure 5 also contains a representative $\bar{u}(\phi, t)$ diagram for the jets in the EXP system, showing their equatorward migration and regeneration in high latitudes; we turn to them next.⁶

b. The EXP jet range

The cases chosen to illustrate the progression of the flow with heating complexity for the EXP structure, E1–E6 in Fig. 4 and Table 2, differ from the LIN set because the jet migration alters the dependence on local heating components. There is no need, for example, for the $P(\phi)$ forms involving two separate baroclinic zones. The $\bar{u}(\phi, t)$ diagram for the E6 case in Fig. 5b is typical and shows the timescales to be about 5000 days between mergers involving the W_2 jet and about 15 000 days for the complete migration of a W_5 jet from high latitudes to its merger with a W_2 jet at 23°S; the latter interval corresponds to a migration speed of 3 cm s^{-1} . The mi-

gration, merger, and renewal of jets also complicates the use of a positional terminology, which is now refined so that W_i refers to the i th westerly jet from the equator at a particular time.

The circulation given by the elementary $P_2(\phi)$ heating distribution consists of five westerly jets plus an E_0 easterly current at the equator, for the E1 case in Fig. 4a. The jets have similar widths, with amplitudes that decrease poleward, and are separated by zones having almost no zonal flow rather than by easterlies. But the jets now reach lower latitudes than their LIN counterparts, with the W_1 jet core settling at 12°S, due in part to the continuous equatorward migration. The migration does not extend to the equator, however, as it is blocked by the E_0 current.

Turning next to the two-zone $P_{\text{BT+BC}}$ heating distribution, we find that for the EXP system the width of the barotropic zone is crucial as it determines whether or not a sufficiently strong E_0 current can develop to stop the migration reaching the equator and forming a W_0 flow. The critical width for the barotropic zone to exclude an equatorial westerly lies somewhere between 6° and 9° of latitude, compared to the 3° to 6° needed by the LIN system with two baroclinic zones. Thus, in the E2 case in Fig. 4b, the westerlies are well blocked

⁶ The reasons for the different behavior of the LIN and EXP systems are discussed in section 5.

by the 12°-wide barotropic zone and the strong E_0 current that it allows. Although the W_1 jet core ends up at 15°S, it initially forms at 10°S, but mergers with migrating W_2 jets at 2000 days and 5500 days, together with the gradually strengthening E_0 current, move the jet poleward.

To produce a westerly current at the equator, the E_0 flow must not be allowed to become too strong. This is so in the E3 case in Fig. 4c where the barotropic zone is only 6° wide, not enough to stop the jets from migrating all the way to the equator even though an E_0 easterly persists there for the first 3000 days. Mergers between the W_1 and W_2 jets at 1500 days and 4500 days produce a westerly current strong enough to displace the E_0 flow. The resulting conditional W_0 westerly at the equator is, however, just a part of the W_1 jet whose core lies at 4°S and, unlike in the LIN cases, does not form a distinctly separate current.

Given that jet migration can overcome the easterlies of a narrower barotropic zone, a one-component P_{BC} heating distribution should produce the same circulation as the E3 case, which is what the E4 solution in Fig. 4d confirms. Again this differs from behavior in the LIN system and again an E_0 current prevails initially until mergers between the W_1 and W_2 jets at 1100 days and 3600 days produce a stronger westerly that spreads to the equator. Details in the $P(\phi)$ heating distribution between the equator and 9°S appear to be of little consequence given the inexorable migration so we can proceed directly to the most complex distribution.

Thus, consider the two cases E5 and E6 in Figs. 4e,f that describe the circulations produced by the complex P_{DIP} distribution. The two cases differ in that E5 has the simpler eddy fluxes while E6 has the stronger heating rate and a deeper equatorial flow. The lengthy E6 calculation extends to 21 000 days to establish the steadiness of the flow configuration when individual jets migrate and regenerate (Fig. 5b). Most jets form quickly but the W_0 current has a longer timescale and takes about 10 000 days to reach its full amplitude; see Fig. 11 later. The midlatitude jets migrate steadily and continuously equatorward but do not penetrate beyond 20°S after the first merger between the W_2 and W_3 jets at 5000 days. An unusual equatorial westerly undercurrent forms in the E6 case at 4000 days and merges vertically with the upper W_0 current at 6000 days to give the deeper flow seen in Fig. 4f.

In general, the jets in the EXP set resemble those in the LIN set when the heating has either the elementary P_2 or the complex P_{DIP} form, despite the extra migration, merger, and regeneration processes. The cool Gaussian dip, in particular, helps create and anchor the more robust tropical currents that limit migration to latitudes poleward of 20°S. Jet migration can be thought of as a form of wave propagation that is blocked at a critical latitude when the tropical currents modify the eigenfunctions appropriately. Such a transfer of energy toward the equator may also be considered as the ultimate turbulent cascade toward a large-

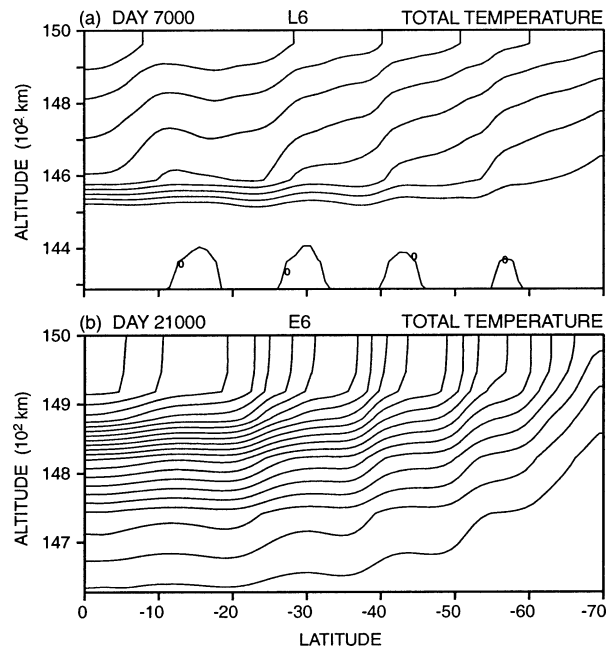


FIG. 6. Meridional sections of the mean total temperature for the L6 and E6 solutions at 7000 days and 21 000 days. In order, the contour interval, maximum, and minimum values are (a) (1, 9.8, 0) °C and (b) (1, 21.4, 0) °C. The values of the related Brunt-Väisälä frequency squared are (a) $1.7 \times 10^{-6} \text{ s}^{-2}$ at the top, $5 \times 10^{-6} \text{ s}^{-2}$ at the interface; and (b) $0.15 \times 10^{-6} \text{ s}^{-2}$ at the top, with a maximum of $1 \times 10^{-5} \text{ s}^{-2}$ at 150 km below.

er scale (Salmon 1998, p. 284). Note, however, that in the EXP solutions of Part II the jets do not migrate, presumably because they are imposed and maintained by a sinusoidal heating that also creates strong easterly currents.⁷

The EXP jets in midlatitudes are almost fully baroclinic as the barotropic component never exceeds 1.5 m s^{-1} anywhere. Although the LIN flows have a more significant (5 m s^{-1}) barotropic contribution, in neither case is it clear what role this plays in determining the jet scales.

4. Steady multiple jets

To define the processes involved in the formation of the steady multiple jets, the time-averaged eddy transports are examined for the two main states realized in the LIN set. The first case, L6 in Figs. 5–9, is considered *realistic* as it displays a Jupiter-like set of jets. Then follows the L1 case, considered *basic* as it involves the elementary $P_2(\phi)$ heating function. These two states mainly differ in low latitudes and their differences help isolate the phenomena that can occur near the equator.

⁷ The E1–E6 potential vorticity distributions are similar to the EXP form seen in Fig. 6 of Part II, but with the stationary dips now replaced by equatorward-moving (escalator) steps.

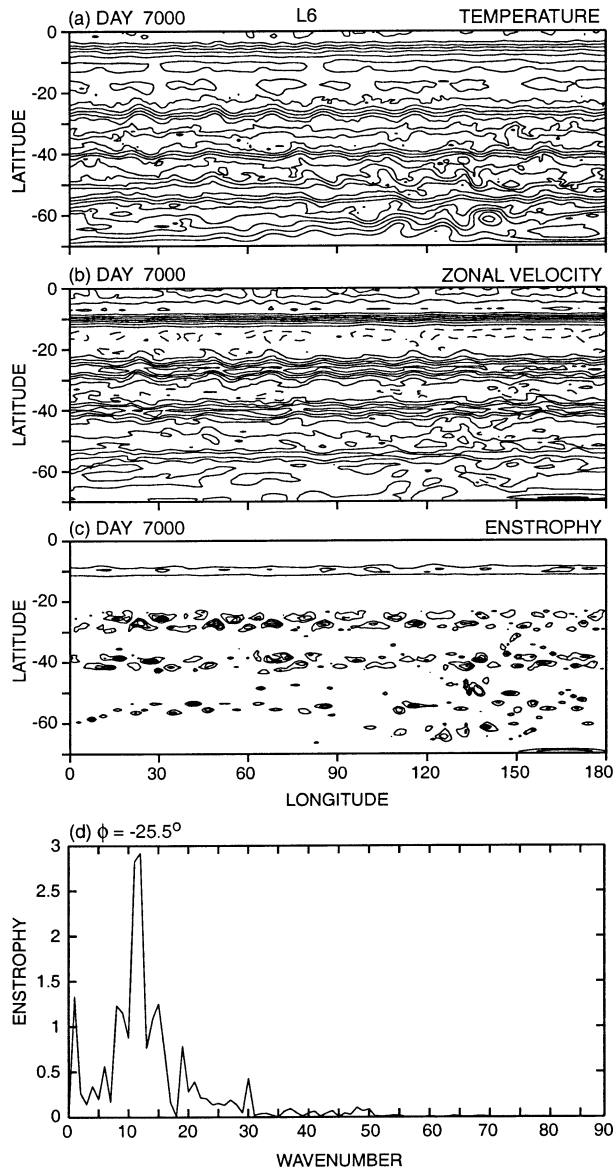


FIG. 7. Horizontal sections of the primary fields for the L6 solution at 7000 days, sampled at a depth of 112 km, together with a spectral analysis of the enstrophy field at $\phi = -25.5^\circ$. In order, the contour interval, maximum, and minimum values are (a) (0.2, 6.1, 0.2) $^\circ\text{C}$, (b) (20, 144, -33) m s^{-1} , and (c) (0.5, 2.6, 0) $\times 10^{-9} \text{ s}^{-2}$, where the enstrophy is the square of the vorticity $\zeta = a^{-1}[v_\lambda - \cos^{-1}\phi(u \cos\phi)_\phi]$.

a. The realistic LIN circulation

The axisymmetric spinup of the L6 system produces a broad westerly flow in midlatitudes and, thanks to the Gaussian cooling dip, a sharp westerly jet of 180 m s^{-1} at 8°S , with a weak easterly flow in between; see the first curve in Fig. 5a. Once perturbed, the broad westerly soon develops baroclinic instabilities that change it completely into three midlatitude westerly jets. The sharp axisymmetric component, however, survives in a modified form as a W_1 jet while its instability helps generate the westerly

at the equator. The original easterly also survives but is broadened by eddy action into an E_1 current.

The equilibrated jets extend 500 km into the fluid and end just below the thermal interface (Figs. 3f and 6a). The fluid remains statically stable everywhere. Although the Brunt–Väisälä stability is strongest at the interface due to the latitudinally varying heating component, the active layer also has a significant value due to the background component.⁸ The zonality of the jets is evident in the horizontal sections, except in high latitudes where β is weak (Fig. 7). The axisymmetric residual of the W_1 jet is most apparent in the enstrophy field, which elsewhere contains eddies lying on both sides of each jet core. The enstrophy eddies are less than 3° wide and become smaller with latitude; in the spectrum for the W_2 jet, they exhibit a peak at wavenumbers $k = 11$ and 12 over the 180° sector. Although the observed eddies are half this scale, their action is reasonably well represented in the L6 solution.

The midlatitude eddy transports in Figs. 8b,c,f reflect the action of three sets of nonlinear baroclinic instabilities, all centered on the cores of the W_{2-4} jets that they sustain at $\phi = (26, 40, 55)^\circ\text{S}$. All transports have the same form within each jet: (a) a strong upward heat flux, $w'T'$; (b) a distinct poleward heat flux, $-v'T'$, that is strongest near the interface and generates the planetary waves that propagate upward and then outward; and (c) an eddy momentum flux, $u'v'$, created by these waves that converges on each jet core in the upper half of the active layer. Although the eddy heat transport peaks within the jets, it remains continuous as it relays the heat poleward across the easterlies; the EXP system differs in this regard. These eddy transports all resemble the classic forms seen in terrestrial GCMs with high rotation rates (Williams 1988) and associated with standard nonlinear baroclinic instabilities. This implies that thin and thick layers can have a common dynamics, that confined layers can have classic modes when created under the LIN formulation.

The Eliassen–Palm flux vector $\mathbf{F} = \{F^{(\phi)}, F^{(z)}\}$ and flux divergence E for the Boussinesq model can be defined following Andrews and McIntyre (1978) as

$$F^{(\phi)} = \left\{ -\overline{u'v'} + \overline{u_z} \frac{\overline{v'T'}}{\overline{T_z}} \right\} \frac{\cos^2\phi}{a} \quad (7)$$

$$F^{(z)} = \left\{ (f + \overline{\zeta}) \frac{\overline{v'T'}}{\overline{T_z}} - \overline{w'u'} \right\} \cos^2\phi \quad (8)$$

$$E = \frac{\partial F^{(\phi)}}{\partial \phi} + \frac{\partial F^{(z)}}{\partial z}, \quad (9)$$

where $\overline{\zeta} = -(a \cos\phi)^{-1}(\overline{u} \cos\phi)_\phi$. The E field is plotted in Fig. 9 for the L6B case (a recreation of the L6 case on a different computer) using contour values that are

⁸ See the caption of Fig. 6 for typical B values.

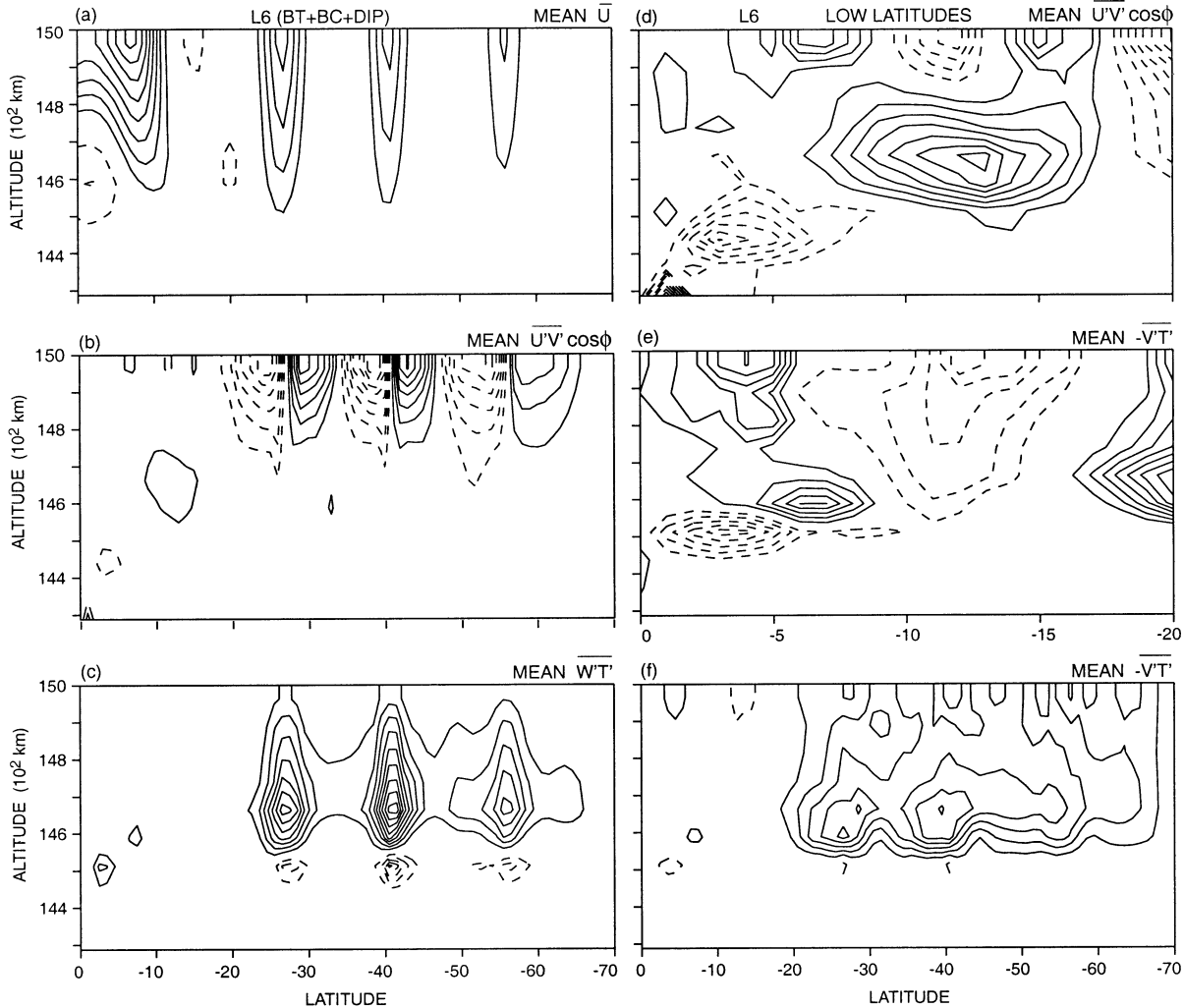


FIG. 8. Meridional sections of the primary eddy transports for the L6 solution. The means are based on daily averages taken over 100–7000 days. The top part of the right-hand column details the weaker low-latitude transports. In order, the contour interval, maximum and minimum values are (a) (20, 166, -41) m s^{-1} , (b) (2, 14.2, -17.9) $\text{m}^2 \text{s}^{-2}$, (c) $(0.2, 1.9, -1.1) \times 10^{-3} \text{ } ^\circ\text{C m s}^{-1}$, (d) $(0.5, 3.7, -5.1) \text{ m}^2 \text{ s}^{-2}$, (e) $(0.5, 3.9, -2.9) \times 10^{-2} \text{ } ^\circ\text{C m s}^{-1}$, and (f) $(0.2, 1.2, -0.3) \times 10^{-1} \text{ } ^\circ\text{C m s}^{-1}$. The zero-value contours are omitted.

powers of 2 to reveal the weaker contributions. The flux divergence is positive within the jet cores due to the $F^{(\phi)}$ term though elsewhere the $F^{(z)}$ term is dominant and the wave propagation mainly upward.

Turning to low latitudes, the tropical eddy transports occur primarily during the first 1000 days and must be plotted separately, on the right side of Fig. 8, to reveal their form. The processes producing these relatively weak transports are multiple and difficult to isolate. In particular, the eddy momentum transport $\overline{u'v'}$ diverges from the jet core at 8°S near the upper surface but also has a stronger component at depth that traverses the jet and transfers momentum equatorward to drive the W_0 current. The baroclinic instability of the W_1 jet, as defined by $\overline{v'T'}$, is centered at 7°S . Some of these transports of momentum and heat are produced by planetary waves emanating from midlatitudes and some are due

to the local baroclinic and barotropic instabilities, but the components are difficult to disentangle. Focusing on a simpler system containing just a single W_1 jet in section 6 gives a clearer view of low-latitude dynamics while the following null case provides a reference state and further perspective.

b. The basic LIN circulation

For the *basic* L1 case with the elementary $P_2(\phi)$ heating in Fig. 10, the two main midlatitude jets W_2 and W_3 have the following standard features: converging $\overline{u'v'}$, localized $\overline{w'T'}$, and peak $\overline{v'T'}$ near the interface. The high-latitude W_4 jet, however, has a poleward traversing $\overline{u'v'}$. But in low latitudes, the W_1 jet centered at 17°S is baroclinically stable, though weak eddies do exist to produce a weak poleward momentum flux across

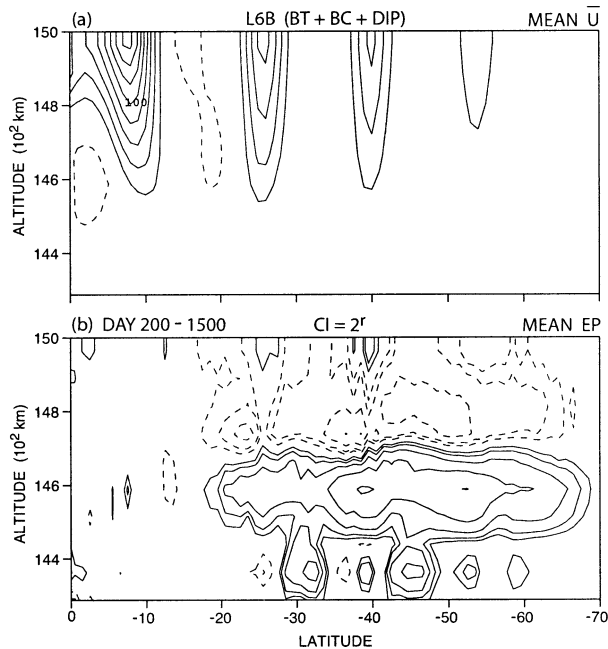


FIG. 9. Meridional sections of the mean zonal velocity and Eliassen–Palm flux divergence, for the L6B solution (an L6 variant). The means are based on daily averages taken over 200–1500 days. (a) The contour interval, maximum, and minimum values are (20, 164, -36) m s^{-1} ; (b) to reveal the weaker contributions, the contour values are based on powers of two, as 5×2^r for $r = (0, 1, \dots, 4)$ plus -5×2^r for $r = (0, 1, 2, 3)$, in units of 10^{-5} m^2 ; the zero-value contours are omitted.

it and support the E_1 current near the equator (Fig. 10d). This W_1 jet is the residual of a broad axisymmetric westerly that has been truncated at 22°S by the currents produced by the midlatitude instabilities.

The L1 case shows that without a significant baroclinicity in low latitudes, the W_1 jet is both too weak to be unstable and too far from the equator to activate a W_0 current. Furthermore, the transitional L4 case shows that even a jet centered at as low a latitude as 10°S is still too far away, even if it is unstable. For the LIN system and the present parameter range, the critical latitude for the W_1 jet to generate a W_0 current lies close to the 8°S value realized by the *realistic* L6 case.

In all cases, the midlatitude jets all have the classic eddy transports normally associated with the nonlinear baroclinic instabilities of thick layers at high rotation rates but that now appear to occur in thin layers as well.

c. Minor LIN variants

To try to isolate the process that determines the scale of the jets, the L1 case can be recalculated using lower and higher baroclinicities, such as $\Delta T = 4^\circ$ and 12°C . These lead, respectively, to six narrower jets with amplitudes of $20 \pm 5 \text{ m s}^{-1}$, and to two wider jets of 50 and 100 m s^{-1} , compared to the original four jets of $50 \pm 10 \text{ m s}^{-1}$. Such values are in keeping with variations

in the Λ , \hat{L}_R , and L_C scales discussed in section 2d, mainly because ΔT also influences the static stability, even though δT is unaltered. Consequently, the variations do not reveal which process actually determines the jet width and amplitude.

5. Migrating multiple jets

To examine the dynamics of the migrating jets in the EXP solutions of Fig. 4, we now consider the *realistic* case E6 in Figs. 11–13 with its Jupiter-like jets. This is followed by the *basic* E1 case with the elementary $P_2(\phi)$ heating to illustrate the main alternative state in low latitudes. The dynamics of the EXP system differs from the LIN due to the jet migration and due to differences in the baroclinic instability character, especially in low latitudes. Because of the jet migration, relatively short (500 day) averaging periods must be used when defining the eddy fields in Figs. 12–14. Longer periods lead to a latitudinal blurring or smoothing of fluxes such as $u'v'$, which move with the jets. Although the standard diagnostics do not reveal the cause of the migration directly because it is such a so slow process, they may expose the symptoms.

a. The realistic EXP circulation

Driven by the complex P_{DIP} heating, the axisymmetric spinup of the E6 system produces a broad westerly flow in midlatitudes plus a sharp westerly of 110 m s^{-1} at 9°S , with a weak westerly flow in between; see the first curve in Fig. 5b. Baroclinic instabilities convert the broad current into four westerly jets and modify the sharp current into a W_1 jet, all within the first 1000 days. The jets immediately begin to migrate equatorward but the W_1 jet stops near 5°S at 5000 days when the first merger of the W_2 and W_3 jets occurs. Further $W_{2,3}$ mergers then follow at 5000-day intervals, each time resulting in a new W_2 jet whose position moves poleward from 17° to 22°S . The blocking of the migration by the W_2 jet allows the W_1 and W_0 currents to develop in relative isolation.

Consequently, the W_1 jet reaches its peak at 6000 days, just after the first $W_{2,3}$ merger, and then remains steady in form while undergoing rapid fluctuations of about $\pm 10 \text{ m s}^{-1}$ in strength (Fig. 11a). Throughout, the W_1 jet has baroclinic and barotropic instabilities whose eddies also produce an equatorial W_0 current that grows fastest over the first 3000 days, then more slowly until 7000 days, after which it undergoes a sharp drop before reaching an oscillatory equilibrium (Fig. 11a). An unusual westerly undercurrent forms at the equator at 4000 days and merges vertically with the developing W_0 current to deepen it at 6000 days; compare Figs. 12a and 12e. This merger accounts for the sharp rise in the barotropic kinetic energy around 7000 days (Fig. 11b).

Given the continuous migration, the meridional struc-

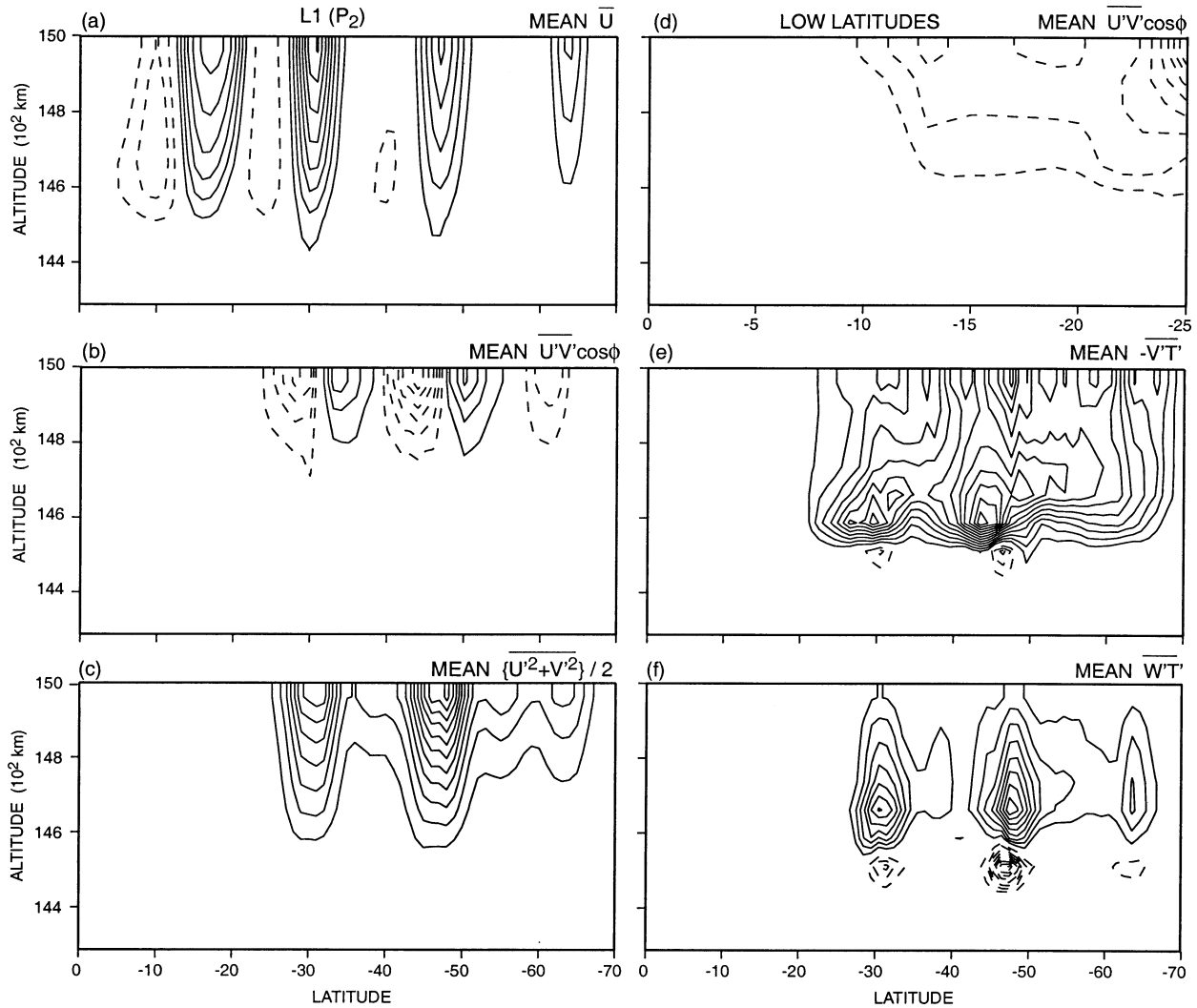


FIG. 10. Meridional sections of the primary eddy transports for the L1 solution. The means are based on daily averages taken over 3500–4000 days. In order, the contour interval, maximum, and minimum values are (a) (10, 81, -27) m s^{-1} , (b) (5, 21.1, -34.1) $\text{m}^2 \text{s}^{-2}$, (c) (50, 568, 0) $\text{m}^2 \text{s}^{-2}$, (d) (1, 0.3, -9.1) $\text{m}^2 \text{s}^{-2}$, (e) (0.2, 2.6, -0.7) $\times 10^{-1} \text{ }^\circ\text{C m s}^{-1}$, and (f) (0.3, 2.7, -2.7) $\times 10^{-3} \text{ }^\circ\text{C m s}^{-1}$. The zero-value contours are omitted.

ture of the circulation shown in Figs. 4f and 12e represents a nonmerging phase only, one in which the three main midlatitude jets extend downward about 200–250 km into the fluid to where the Brunt–Väisälä stability peaks (Fig. 6b). Only the equatorial current reaches the base of the heated layer at the 400-km depth, and then only after merging with the undercurrent. The near-neutral stability layer occupying the top 100 km occurs because the background static stability cannot compensate for the cooling created by the (d/dz) sech(Nz') distribution used to produce a vanishing shear at the top surface. Despite this near-neutral layer, baroclinic instabilities occur at all latitudes, as might be expected from Fjortoft’s (1951) theory.

Turning to the E6 eddies, Figure 12 displays the various transports for both the early formative phase (on the left side) and the steady configuration phase (on the

right side). At all times, the eddy transports lie primarily within the near-neutral 100-km-deep layer, for which the deeper nonzero B field may be acting as a broad thermal interface. Extending only 50 km down, the eddy momentum transport $\overline{u'v'}$ is even shallower yet still responsible for the 200-km-deep jets on which it converges in midlatitudes. During the early phase, the $\overline{u'v'}$ flux in Fig. 12b has an equatorward component that traverses the W_1 jet to produce the W_0 superrotation, but it eventually alters in Fig. 12f to converge on the W_1 jet core as the W_0 flow equilibrates.

The E6 poleward eddy heat transport $-\overline{v'T'}$ in Figs. 12c,g differs markedly from the LIN version as it is discontinuous within the jets and continuous between them,⁹ while being more uniform with height due to the

⁹ The profile for the E1 case in Fig. 14e shows this more clearly.

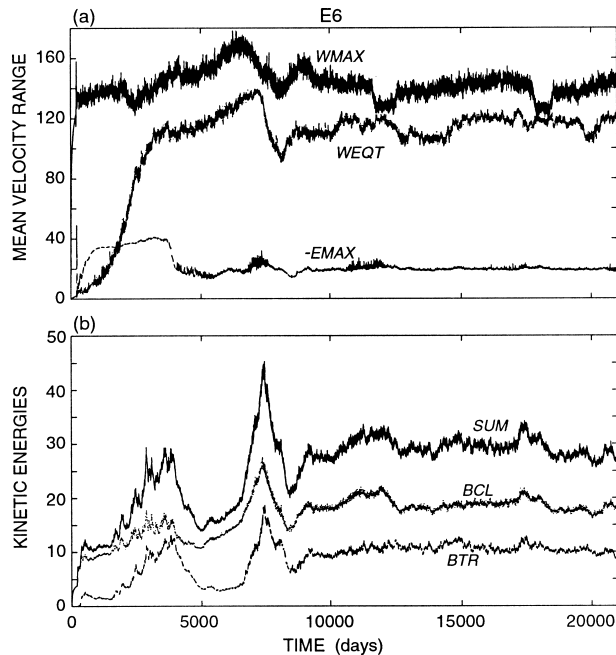


FIG. 11. Diagnostic transients for the E6 solution: (a) the mean westerly and easterly flow extrema in low latitudes and at the equator, where $W_{MAX} = W_1$, $E_{MAX} = E_1$, and $WEQT = W_0$ in $m s^{-1}$; (b) the global mean kinetic energies, $0.5(u^2 + v^2)$ in $m^2 s^{-2}$, showing the total and individual baroclinic (BCL) and barotropic (BTR) components.

neutral stability layer. This transport gradually weakens in low latitudes as the flow approaches equilibrium. The $v'T'$ flux dominates the Eliassen–Palm field in Fig. 13, suggesting that upward momentum transport and its unusual peaking between the jets may also contribute to their migration. However, the Eliassen–Palm field may not be a good measure of processes when a near-neutral static stability exists. According to the vertical eddy heat transport $w'T'$ in Figs. 12d,h, the W_1 jet remains baroclinically unstable throughout, though this instability becomes more confined to the poleward flank of the jet during the later phase.

In the E5 realistic case, with its weaker P_{DIP} heating, the resulting jets and eddy fields are found to be similar to those of the early phase of E6 but to lack the complications caused by the westerly equatorial undercurrent. This means that simple W_0 currents can form as readily in the EXP system as in the LIN setup. Generally, the baroclinic instabilities that occur in the EXP system seem to be close to the classic form, but in low latitudes the eddy transports and their variation between the early and late phases are novel, as is the jet migration in midlatitudes.

b. The basic EXP circulation

The basic state given by the elementary $P_2(\phi)$ heating function for the EXP system, E1 in Fig. 14, consists of five jets of comparable width at 2000 days. No mergers have occurred as yet but a slow migration is underway,

with the W_2 jet, for example, having moved to 24°S from its original position at 30°S. The W_1 jet is an exception, however, and remains at 12°S, which, when compared to the 18°S position of its L1 counterpart, shows that the EXP structure allows baroclinic instability to occur in significantly lower latitudes than does the LIN system. But at the equator, an easterly exists to prevent the W_1 jet, unstable though it may be, from ever generating a W_0 current. To achieve a superrotation, even the EXP system requires more baroclinicity in low latitudes than $P_2(\phi)$ provides.

The variation of the EXP circulations with latitude is most clearly seen in the E1 solution, and shows that while the jets extend 200–300 km into the fluid and become shallower with increasing latitude, the corresponding baroclinic instabilities (as defined by the eddy heat fluxes) extend 70–100 km in depth and become deeper with latitude (Fig. 14). All of the jets have converging eddy momentum transports while the eddy heat transports differ significantly from their LIN counterparts; the eddies transport heat poleward between the jets but not across them (Fig. 14e). The eddies are strongest and deepest in the W_3 and W_4 jets but the jets themselves decrease poleward in amplitude while keeping their widths constant. All of these features of the multiple jets and their instabilities may contain clues as to how they actually arise, set their scale, sustain themselves, and migrate.

Concerning the cause of the migration, closer inspection of the eddy momentum transports reveals that although the $u'v'$ transports converge on the jet cores, the equatorward flux in each jet is significantly stronger than the poleward flux, while the related $u'w'$ transports are almost entirely downward and confined to the poleward side of each jet (Fig. 14b). This is in sharp contrast with the LIN flows where these fluxes are highly symmetrical about each jet core. The associated mean meridional flow mainly consists of Ferrel cells centered on the jet cores. Because cause and effect cannot be distinguished, we can only speculate that these asymmetries in effect imply that the eddies act through $u'w'$ or the $F^{(z)}$ Eliassen–Palm flux to reduce the jet at a given location and through $u'v'$ or $F^{(\phi)}$ to push it equatorward. Presumably, the real origin of the migration lies in the basic character of the baroclinic instabilities and wave dispersion favored by the EXP system, though the weakness of the process makes it difficult to detect.

To summarize, we see that the EXP system favors slowly migrating jets driven by baroclinic instabilities that occur as readily in low latitudes as in midlatitudes. When the baroclinicity extends into latitudes lower than 9°S the barotropic instability of the resulting W_1 jet can lead to an equatorial superrotation. In such cases, the jet migration only reaches 20°S and thus does not directly influence the W_0 onset or maintenance.

6. Equatorial jets

The generation of the W_0 equatorial superrotation in the L6 case discussed above involves low-latitude bar-

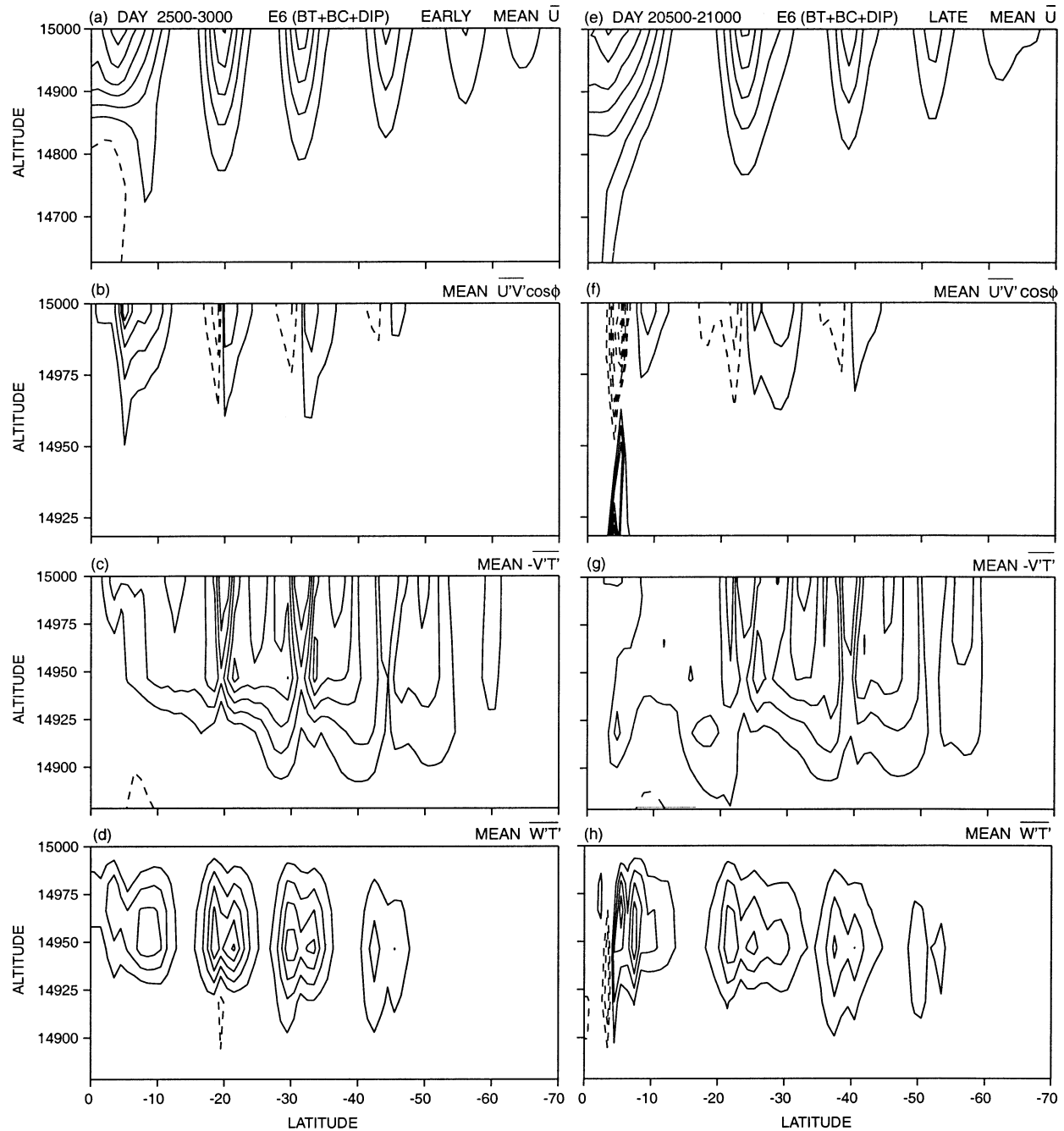


FIG. 12. Meridional sections of the primary eddy transports for the E6 solution. The means are based on daily averages taken over an early phase, 2500–3000 days, on the left side, and over a late phase, 20 500–21 000 days, on the right side. In order, the contour interval, maximum, and minimum values are (a) (20, 135, -39) m s^{-1} , (b) (20, 120, -62) $\text{m}^2 \text{s}^{-2}$, (c) (1, 5.9, -1.2) $\times 10^{-1} \text{ } ^\circ\text{C m s}^{-1}$, (d) (1, 5.2, -1.6) $\times 10^{-3} \text{ } ^\circ\text{C m s}^{-1}$, (e) (20, 144, -15) m s^{-1} , (f) (20, 139, -140) $\text{m}^2 \text{s}^{-2}$, (g) (1, 5.3, -1.2) $\times 10^{-1} \text{ } ^\circ\text{C m s}^{-1}$, and (h) (1, 4.8, -2.9) $\times 10^{-3} \text{ } ^\circ\text{C m s}^{-1}$. The zero-value contours are omitted.

oclinic and barotropic instabilities whose characteristics are complicated by planetary waves emanating from the midlatitude instabilities. To isolate the low-latitude instability more clearly, consider now a more limited LIN system, Q1 in Table 3, for which the heating creates only a W_1 jet in a narrower channel. Creating a single

jet at 8°S then leads to a well-defined instability whose features have much in common with those of the L6 case and also with the EXP system in low latitudes.

Given that the low-latitude instabilities in the two structures have similar momentum transports, the question arises as to whether the W_0 onset depends crucially

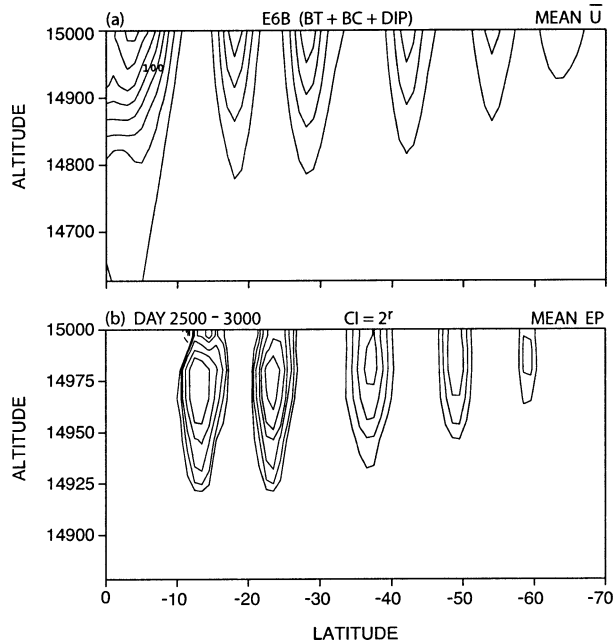


FIG. 13. Meridional sections of the mean zonal velocity and Eliassen–Palm flux divergence, for the E6B solution (an E6 variant). The means are based on daily averages taken over 2500–3000 days. (a) The contour interval, maximum, and minimum values are (20, 169, -11) m s^{-1} ; (b) to reveal the weaker contributions, the contour values are based on powers of two, as 5×2^r for $r = (0, 1, \dots, 5)$ plus -5×2^r for $r = (0, 1, 2, 3)$, in units of 10^{-2} m^{-2} ; the zero-value contours are omitted.

on the active layer being thin and confined, or whether such superrotations can also occur in thick or terrestrial atmospheres. On switching from Jovian to terrestrial parameters (Table 3), we find that the classic baroclinic instability seen in a reference case, Q2, can be replaced by a quite different mode in which the barotropic and baroclinic instabilities generate a W_0 current in the Q3 solution. This new form of instability defines the essence of the equatorial process.

a. Jovian superrotation

To create a solitary low-latitude jet centered at 8°S , the fluid is subjected to a simple linear heating with a constant baroclinicity extending from 3° to 15°S , as in form 6 of Fig. 2. The 2.2°C heating amplitude used for Q1 leads to W_1 and W_0 flows with peaks of 214 and 187 m s^{-1} , respectively, in Fig. 15, whereas a 2.0°C heating produces winds of 168 and 69 m s^{-1} , in which W_0 is much reduced. This indicates that for the Q1 configuration to occur, the W_1 jet must reach a critical value close to 150 m s^{-1} before its instability can generate a significant W_0 flow.

In the Q1 solution, the W_0 current grows quickly to 50 m s^{-1} from the W_1 instability but then increases in steps (Fig. 15a) before leveling off at 10 000 days; later, the two westerlies merge into a single current (Fig. 15c).

During the W_0 growth phase, the eddy amplitudes lie in the $30\text{--}40 \text{ m s}^{-1}$ range for about 7000 days but then rapidly decay, allowing the zonal current to equilibrate (Fig. 15b). Apparently, the eddies drive the W_0 current until it approaches W_1 in strength, at which point the currents equilibrate by eliminating the eddy source.

When averaged over the growth phase, the mean zonal flow in the Tropics has the same form as in the L5 and L6 multijet cases (Figs. 16a and 3e,f), but toward the end of the calculation the contours become flatter and the W_0 and W_1 components are indistinguishable (Fig. 15c).¹⁰ The eddy heat transports produced by the instability peak just above the interface in the W_1 core at 7°S and extend to within 3° of the equator (Fig. 16e,f). The eddy kinetic energy and eddy momentum transport, however, are strongest farther away from the equator in the jet flank at $|\phi| > 10^\circ$ and are produced by waves generated by the instability (Fig. 16b,d).

Over the complete growth phase, the eddies mainly transport momentum equatorward across the cyclonic part of the W_1 jet between 8° and 18°S (Fig. 16b). But when averaged over the 300–800-day period of rapid W_0 growth, the $u'v'$ field displays a significant second component in a 200-km layer that extends from 10°S to the equator, together with the main 400-km-deep contribution (Fig. 16c). This second component drives the W_0 current and is produced by the barotropic instability of the equatorward flank of the W_1 jet. Looking back to the $u'v'$ field for the L6 case in Fig. 8d in light of the distribution for Q1, we now see that most of the distribution in the Tropics can be attributed to the W_1 instability if we assume that the weak poleward contribution that disrupts the predominantly equatorward transport near the upper surface is accredited to externally generated planetary waves.

b. Terrestrial superrotation

To examine the onset of W_0 currents in a terrestrial context, we now impose heating distributions with $\cos^n\phi$ profiles to create jets that lie in mid- or low latitudes, depending on the value of n . This section considers the two solutions produced by $n = 2$ for the Q2 case and by $n = 8$ for the Q3 case. The terrestrial parameters are listed in section 2b and Table 3 for the solutions plotted in Figs. 17–19. The dynamical processes involved are discussed in greater detail for a more realistic model in Williams (2003a).

The axisymmetric states created during the spinup of the Q2 and Q3 solutions have similar forms but differ from those of the standard theory (Held and Hou 1980) in that the jet core and the Hadley cell limit lie near 20°S for the 70°S domain rather than at the 30°S location produced by the standard $P_2(\phi)$ heating. When the two

¹⁰ Note that, after 10 000 days, $W_1 > W_0$ in Fig. 15a when the velocities are sampled at all heights, while $W_1 = W_0$ in Fig. 15c when sampled at a fixed height.

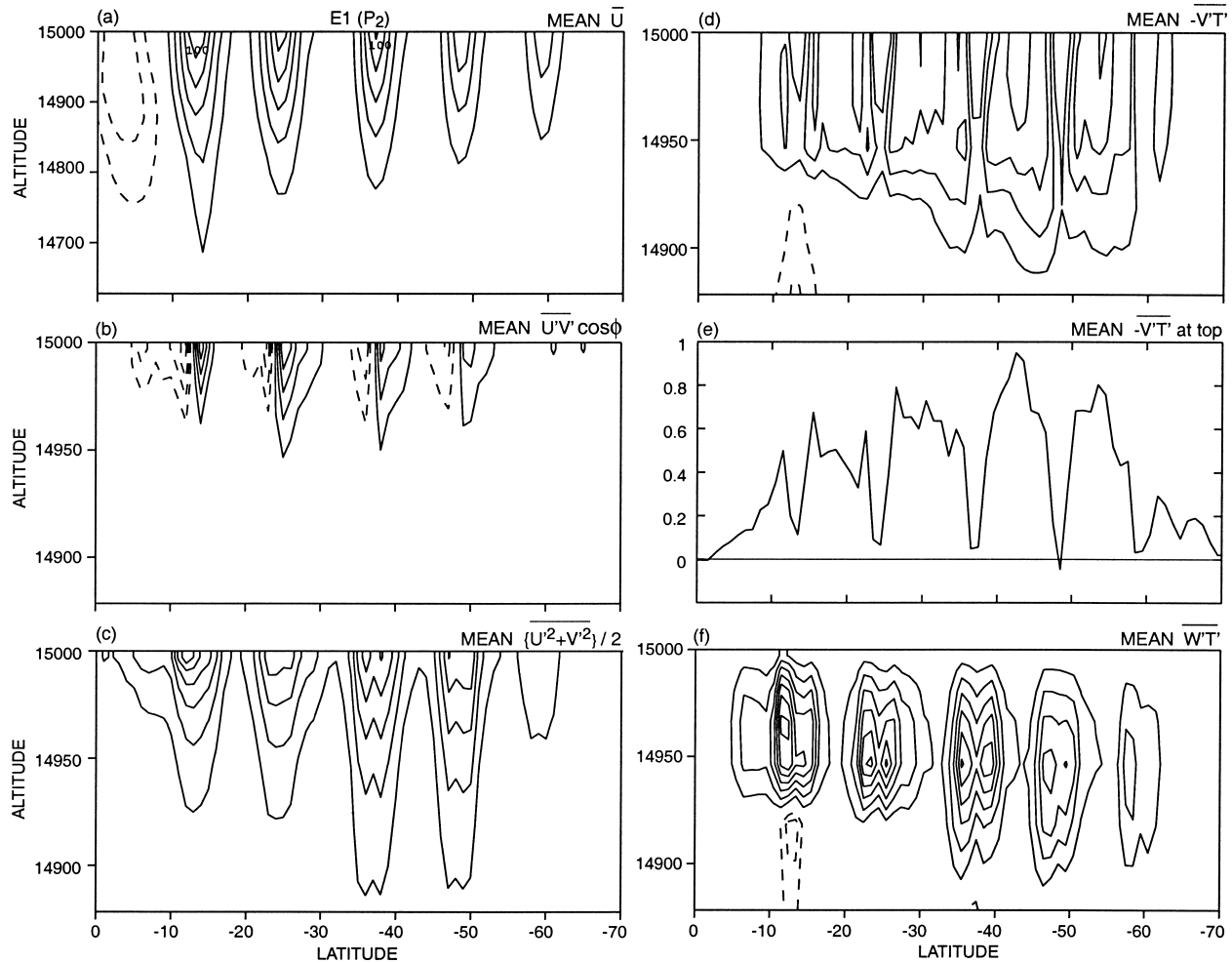


FIG. 14. Meridional sections of the primary eddy transports for the E1 solution. The means are based on daily averages taken over 1950–2000 days. In order, the contour interval, maximum, and minimum values are (a) (20, 116, -57) m s^{-1} , (b) (20, 100, -82) $\text{m}^2 \text{s}^{-2}$, (c) (100, 687, 1) $\text{m}^2 \text{s}^{-2}$, (d) (2, 10, -4.3) $\times 10^{-1} \text{ }^\circ\text{C m s}^{-1}$, (e) (9.5, -0.5) $\times 10^{-1} \text{ }^\circ\text{C m s}^{-1}$, and (f) (1, 7.3, -2.6) $\times 10^{-3} \text{ }^\circ\text{C m s}^{-1}$. The zero-value contours are omitted.

axisymmetric states are perturbed, Q2 develops a standard circulation in Fig. 17 while Q3 has a novel circulation with an equatorial superrotation in Fig. 18. This simple switch in regimes as the baroclinic zone moves to lower latitudes occurs most readily when the flows start from a fully formed axisymmetric state whose jet lies in low latitudes. The novel regime may be less pervasive than the classic state but, nevertheless, exhibits a permanent superrotation, a mode related to those described by Suarez and Duffy (1992) and Saravanan (1993), despite differences in the forcing.

The standard Q2 circulation that forms the reference state in Fig. 17 has all the classic features seen in dry GCM circulations (cf. Williams 1988, Figs. 16c–26c). According to the eddy heat transports, the baroclinic instability occurs within the jet core, between 30° and 40°S , with $\overline{v'T'}$ peaking near the ground but extending aloft while $\overline{w'T'}$ is strongest at midlevels, as expected.

Waves propagating upward from the instability transport momentum upward to give a peak $\overline{u'w'}$ aloft before propagating equatorward to give the peak $\overline{u'v'}$ at 30°S . The eddies act to maintain the jet poleward of its axisymmetric position, at the latitude where the eddy kinetic energy also peaks. The Eliassen–Palm flux divergence and vectors (Fig. 19a) are consistent with the standard view given by nonlinear baroclinic instabilities (Edmon et al. 1980), in which waves propagate upward and then equatorward, thereby transporting westerly momentum poleward.

On the other hand, the novel Q3 circulation in Fig. 18 differs in almost all aspects from the standard form. The most original feature, the equatorial superrotation, grows immediately as the axisymmetric state is perturbed, but does so quite slowly over 500 days. Elsewhere, the jet and the thermal front now form in low rather than middle latitudes, near 20°S , and weak east-

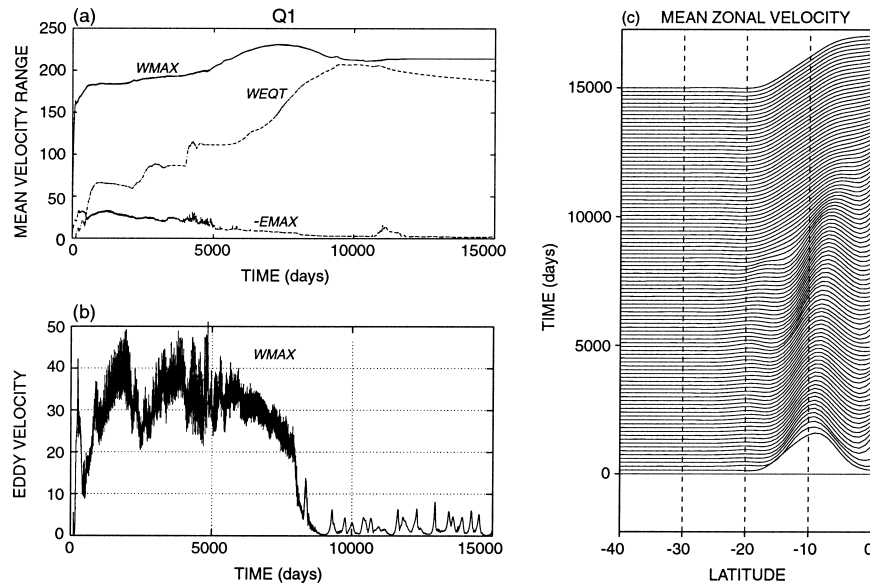


FIG. 15. Diagnostic transients for the Q1 low-latitude solution: (a) the mean westerly and easterly flow extremes, sampled at all heights for low latitudes and the equator, where $W_{MAX} = W_1$, $E_{MAX} = E_1$, and $W_{EQT} = W_0$ in $m\ s^{-1}$; (b) the eddy westerly maximum in low latitudes in $m\ s^{-1}$; (c) time section of the mean zonal velocity sampled near the top surface with a scale for the maximum of $207\ m\ s^{-1}$ that is equivalent to 15 times the vertical spacing between the curves.

erlies fill the region poleward of $35^\circ S$. The meridional circulation is strongly influenced by the instability, with the Hadley cell becoming smaller, much weaker, and significantly constrained by a Ferrel cell of comparable strength.

According to the Q3 eddy heat transports, the novel baroclinic instability is centered in low latitudes and confined to lower levels (Figs. 18f,g). The eddy momentum transport $\overline{u'v'}$ is mostly equatorward and, although there is a small convergence on the jet core, it essentially pushes through to the equator at midlevel to drive the W_0 current. The vertical eddy momentum flux, upward at the equator, also supports the W_0 current but is mostly downward in the jet flank. The Eliassen–Palm flux divergence is positive aloft, in keeping with the production of eddy-driven zonal flows by upward-propagating waves (Fig. 19b). The weaker E flux divergence and F flux vectors in low latitudes (Fig. 19c) reveal the existence of an equatorward wave propagation at low levels together with a poleward propagation aloft, if the eddies are wavelike. The role of such processes in the equatorial superrotation is discussed in Williams (2003a).

The scale of the eddies, as defined by a spectral analysis of the enstrophy at the top surface, is not too different between the two states, with a maximum wavenumber of $k = 4$ over a 180° sector in both cases.

7. Easterly and hexagonal jets

To complete the set of circulations, consider now a couple of simple variations on the above theme that may

be of singular planetary relevance. The first variant shows how *easterly* currents can be generated by elementary heating arrangements. The solutions discussed above are notable for their lack of significant easterly currents and although this may be reasonable for Jupiter and Saturn, it is not valid for Neptune where a strong easterly current occupies the equatorward half of each hemisphere. But by removing the a priori assumption that the active layer have a constant depth and by allowing the layer to deepen toward the pole, simple easterly currents can be readily realized. The P1 and P2 cases examine these novel easterlies in the EXP system for the axisymmetric and three-dimensional states, respectively. The second variant, the P3 case, involves minor parameter changes in the LIN system but yields a circulation with hexagonal jets of possible relevance to Saturn.

a. Easterly currents

To create an active layer whose depth increases with latitude, the confinement rate N of the exponential system is made to decrease with latitude in the baroclinic part of the heating function (2) but not in the background static stability, so that

$$T_r = \Delta T P_2(\phi) \exp[N(\phi)z'] + \delta T \exp(N_0 z'), \quad (10)$$

where $N(\phi) = N_0/[1 + d(0.5 - P_2)]$ varies from 400 to 100 between 0° and $45^\circ S$ when $N_0 = 100$ and $d = 1.5$, where d is the depth variation parameter (Table 3). The $N(\phi)$ variation can be interpreted as implying either that (a) the penetration depth of the external heat source

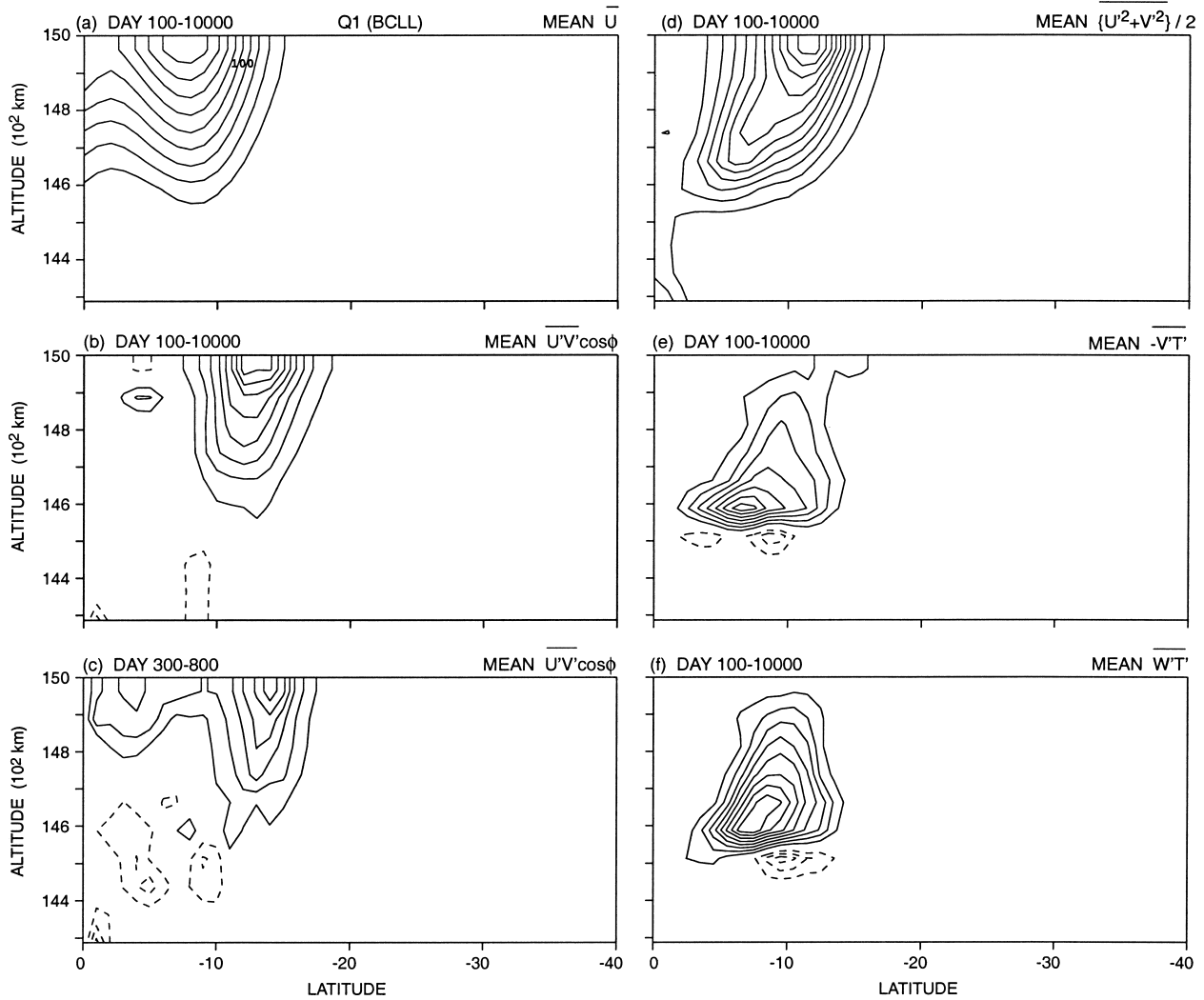


FIG. 16. Meridional sections of the primary eddy transports for the Q1 low-latitude solution. The means are based on daily averages taken over 100–10 000 days for most items, but (c) over 300–800 days. In order, the contour interval, maximum, and minimum values are (a) (20, 196, -6) m s⁻¹, (b) (1, 8.6, -2.4) m² s⁻², (c) (1, 6.7, -3.3) m² s⁻², (d) (20, 231, 0) m² s⁻², (e) (1, 7.8, -2.8) × 10⁻² °C m s⁻¹, and (f) (1, 8.8, -3.6) × 10⁻⁴ °C m s⁻¹. The zero-value contours are omitted.

increases with latitude, or (b) the depth at which the internal heat source becomes effective increases with latitude.

Although a monotonic heating is imposed on the fluid by $P_2(\phi)$ in (10), it extends over different depths at different latitudes and can, when d is large enough, produce a negative baroclinicity in lower latitudes and a positive baroclinicity in higher latitudes; these in turn can produce, through the thermal wind balance, an easterly and westerly current in the two regions, such as those seen in the axisymmetric P1 solution in Fig. 20. A reverse (Ferrel) cell forms between the equator and 25°S and advects heat downward to deepen the thermal layer, which elsewhere corresponds closely to the heating function. Consequently, the active layer has only a modest increase in depth between the equator and 45°S, according to the temperature field.

The extent of the easterly current, as defined by the thermal wind associated with T_r , is given by the latitudinal heating gradient:

$$\frac{\partial T}{\partial \phi} = \Delta T \exp[N(\phi)z'] \frac{\partial P_2}{\partial \phi} \left\{ 1 + \frac{P_2 d N_0 z'}{[1 + d(0.5 - P_2)]^2} \right\}, \tag{11}$$

where z' in the last term provides the only negative factor for reversing the baroclinicity in lower latitudes. The line along which the baroclinicity given by (11) vanishes¹¹ matches the zero zonal flow contour in Fig. 20a to within 3° of latitude, except near the upper surface where the Ferrel cell is influential.

¹¹ The P_2 profile is normalized over 80°.

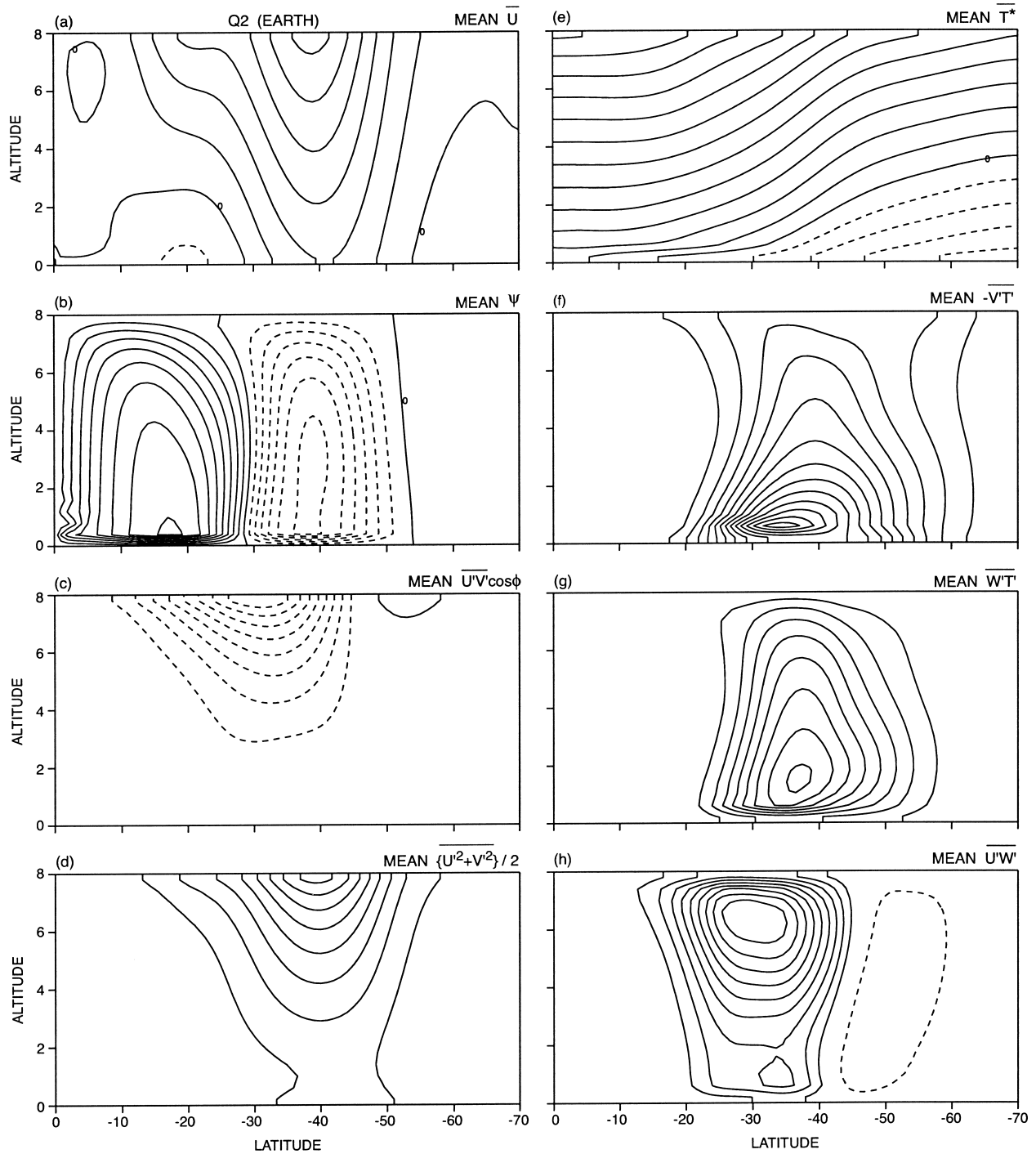


FIG. 17. Meridional sections of the primary fields and eddy transports for the Q2 solution with terrestrial parameters. The means are based on daily averages taken over 500–1000 days. In order, the contour interval, maximum, and minimum values are (a) (4, 25, -5) m s^{-1} , (b) (5, 40.7, -31.6) $\times 10^2 \text{ m}^2 \text{ s}^{-1}$, (c) (2, 2.8, -17.9) $\text{m}^2 \text{ s}^{-2}$, (d) (10, 83, 0) $\text{m}^2 \text{ s}^{-2}$, (e) (4, 48, -18) $^\circ\text{C}$, (f) (0.5, 6.8, -0.2) $^\circ\text{C m s}^{-1}$, (g) (0.5, 4.1, -0.1) $\times 10^{-3} \text{ }^\circ\text{C m s}^{-1}$, and (h) (1, 9.8, -1.9) $\times 10^{-3} \text{ m}^2 \text{ s}^{-2}$. The zero-value contours are omitted for the eddy fields.

Clearly, variations in the depth to which the heating penetrates (or originates at) can influence a latitudinally monotonic distribution to the extent that they reverse the baroclinicity and zonal wind in lower latitudes. The depth variations needed to do this are not extreme and

so perhaps could be realized on a planet. The zonal flow found on Neptune (Limaye and Sromovsky 1991) has some features in common with the P1 solution, although the planet also has strong easterlies at the equator.

To examine the stability of the axisymmetric P1 cir-

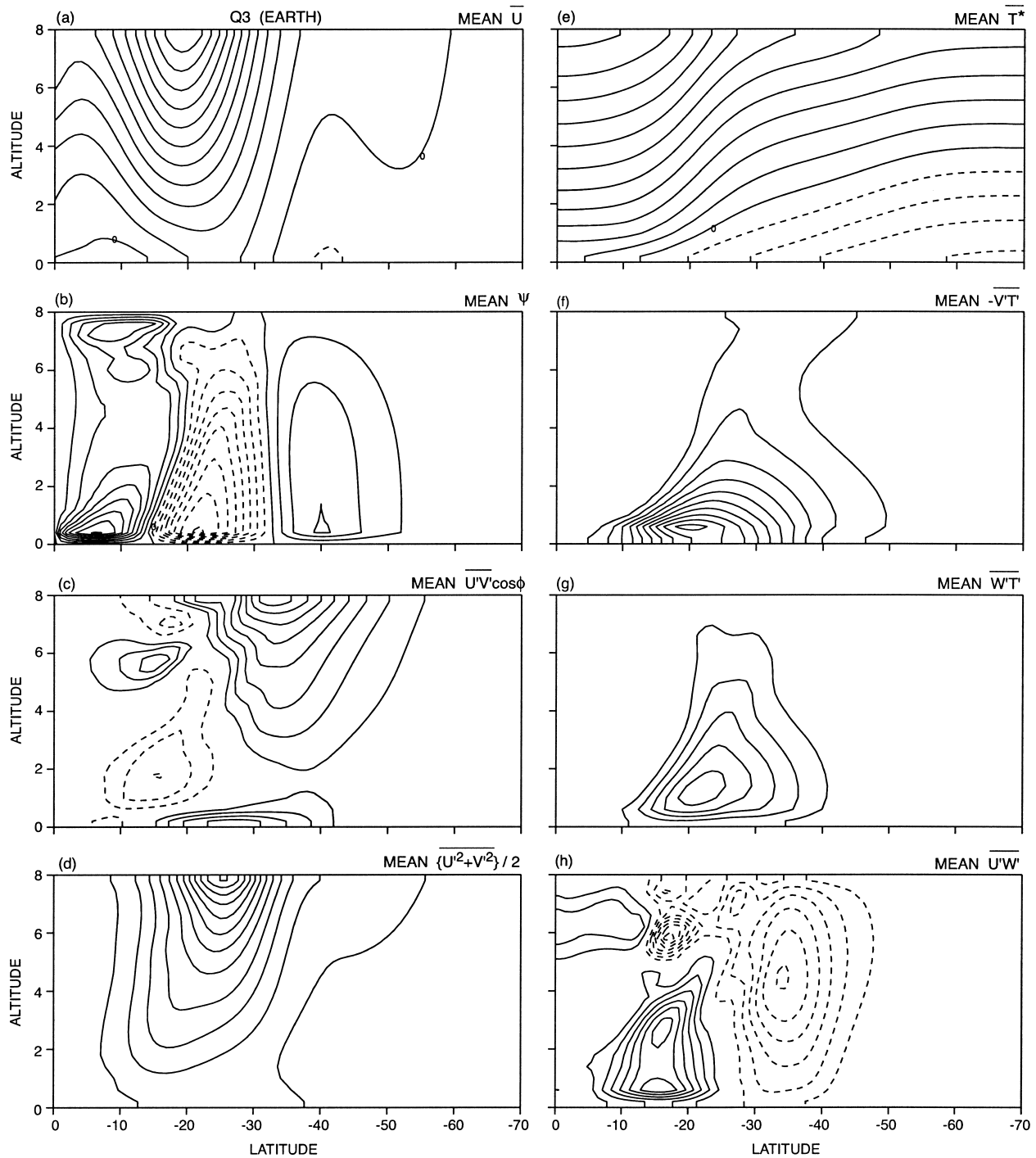
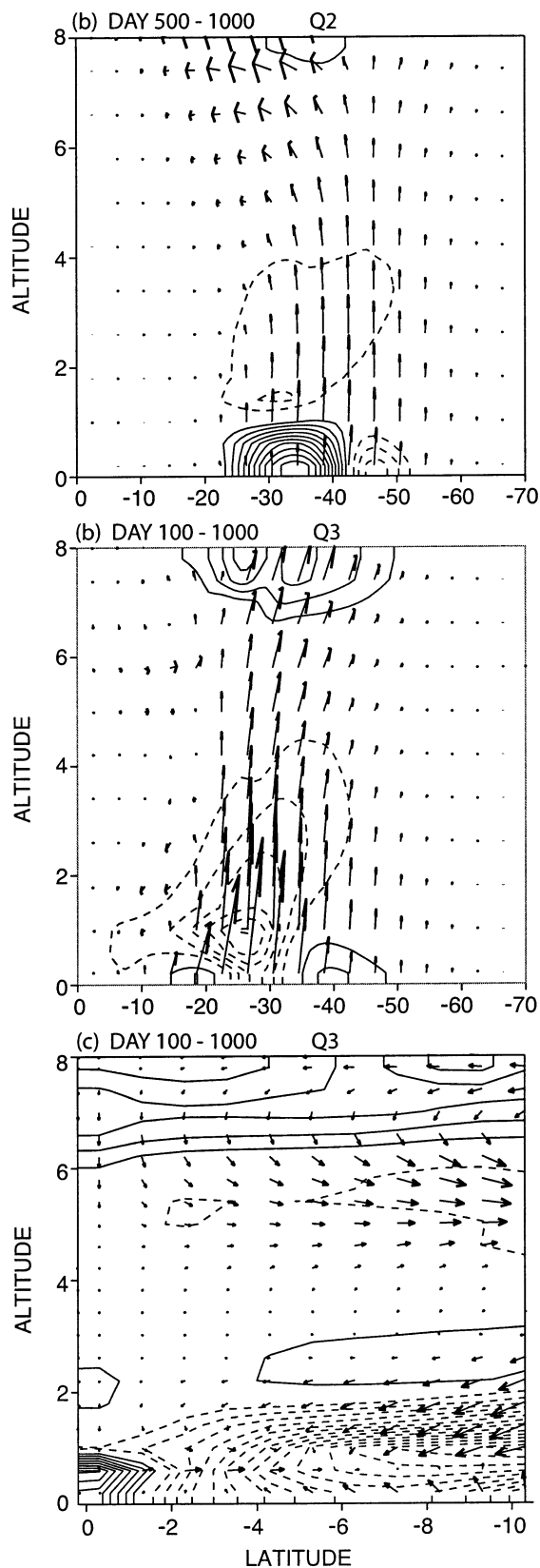


FIG. 18. Meridional sections of the primary fields and eddy transports for the Q3 solution with terrestrial parameters. The means are based on daily averages taken over 100–1000 days. In order, the contour interval, maximum, and minimum values are (a) (4, 48, -4) m s^{-1} , (b) (5, 40.4, -40.5) $\times 10 \text{ m}^2 \text{ s}^{-1}$, (c) (1, 8.6, -3) $\text{m}^2 \text{ s}^{-2}$, (d) (10, 120, 0) $\text{m}^2 \text{ s}^{-2}$, (e) (4, 45, -16) $^{\circ}\text{C}$, (f) (1, 10.4, -0.4) $^{\circ}\text{C m s}^{-1}$, (g) (1, 5.6, -0.8) $\times 10^{-3} \text{ }^{\circ}\text{C m s}^{-1}$, and (h) (1, 6.9, -7.5) $\times 10^{-3} \text{ m}^2 \text{ s}^{-2}$. The zero-value contours are omitted for the eddy fields.

ulation, a three-dimensional calculation is made for the related P2 system. The resulting solution in Fig. 21 shows that small-scale baroclinic instabilities arise at 10° and 50°S that are weak in the easterly current but strong in the westerly. Because the eddies are small and

weak, the original broad easterly and westerly currents remain intact and provide the dominant mode.

The eddies in the westerly produce two small-scale minijets within the main current. The singular peak in the eddy kinetic energy and the unusually narrow eddy



heat transport $\overline{v'T'}$ both suggest the action of a single instability. But the bimodal eddy momentum transport $\overline{u'v'}$ is more symptomatic of two instabilities. Specifically, the $\overline{u'v'}$ field shows that the eddies converge momentum on the two minijet cores. Elsewhere, the eddies in the easterly current are simpler: the poleward traversing $\overline{u'v'}$ and the positive $\overline{w'T'}$ are consistent with the standard form of baroclinic instability, while the equatorward eddy heat transport is novel but simply due to the reversal of the baroclinicity in low latitudes (cf. Feldstein 1991).

As regards any planetary application, the minijets and other three-dimensional features introduced by the baroclinic instabilities could be eliminated or enhanced by altering the background static stability.

b. Hexagonal currents

Finally, consider a solution P3 in Fig. 22 that displays a feature of singular planetary relevance. For this case, we return to the LIN system and make a slight variation in the L6 parameters (Table 3). The usual five-jet circulation develops, but when this is viewed in a polar projection, some jets take on a hexagonal form that lasts for about 100 days, first in the W_3 jet at 55°S and 500 days, and then in the W_2 jet at 30°S and 600 days. The calculation uses a 60° sector and this no doubt influences the existence and order of the polyhedron that occurs. The hexagonal appearance is actually due to a localized nonlinear wave that occurs within the jets near the middle of each sector.

The nonlinear wave is associated with concentrated heat fluxes: the $\overline{v'T'}$ field is sharp and deep, while the $\overline{w'T'}$ field is very narrow, intense, and unusually deep in each hexagonal jet. On the other hand, the eddy momentum transports are of the standard converging form. In reporting the discovery by the *Voyager* spacecraft of a similar hexagonal pattern on Saturn at 70°N , Allison et al. (1990) interpret it as being due to a stationary Rossby wave. Here it is a feature of a nonlinear baroclinic instability that also involves planetary waves. The existence of the hexagonal jets provides a further test on the relevance of the thin layer hypothesis.

8. Conclusions

Multiple jets can be generated and maintained in thin layers when their primitive equation representation is subject to a simple but appropriate Newtonian heating function. Heating functions designed to produce a glob-

FIG. 19. Meridional sections of the Eliassen-Palm flux divergence and vectors for the Q2 and Q3 terrestrial cases. (c) The weak low-latitude contributions are plotted separately for the Q3 case. The contour interval for E and the maximum values of $F^{(a)}$ and $F^{(c)}$ are, in order, (a) (1, 51, 12), (b) (0.5, 10, 9), and (c) (0.05, 1.2, 0.5), in units of 10^{-3} m^2 . The zero-value contours are omitted.

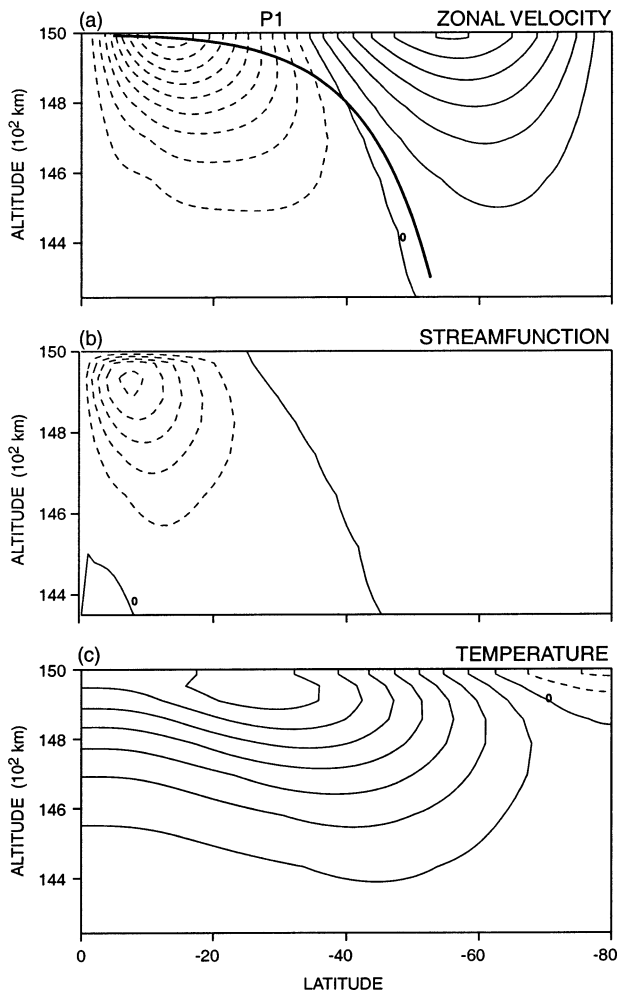


FIG. 20. Meridional sections of the primary fields for the axisymmetric P1 solution for a variable depth layer at 5000 days. The thick line represents the zero value of the theoretical thermal wind given by (11). In order, the contour interval, maximum, and minimum values are (a) (5, 30, -48) m s^{-1} , (b) (0.5, 0.3, -2.6) $\times 10^3 \text{ m}^2 \text{ s}^{-1}$, and (c) (1, 7.7, -2.2) $^{\circ}\text{C}$.

ally uniform baroclinicity lead to a broad axisymmetric westerly flow that can be baroclinically unstable when confined to a thin upper layer by either an exponential (EXP) or locally linear (LIN) vertical heating structure. Broad unstable westerlies evolve into multiple westerly jets that achieve a steady state in the LIN system but only a steady configuration in the EXP system where they migrate continuously equatorward and regenerate in high latitudes. All jets are zonally aligned due to the smallness of the eddies but can occasionally, due to nonlinear waves, appear to be hexagonal (or polyhedral) when viewed in a polar projection. Boosting the baroclinicity in low latitudes helps generate tropical jets whose barotropic instability can, in turn, lead to equatorial westerlies. Such superrotations do not depend on the layer being thin and may, for example, also be generated for Earth's atmosphere provided that the circu-

lation is developed by perturbing a strong axisymmetric state whose jet lies in the Tropics. Most solutions are marked by a lack of significant easterly currents but these too can be generated if the heating is allowed to penetrate to, or originate at, depths that increase with latitude.

Flows in the confined linear (LIN) system behave very much like those in a deep linear system as the eddy transports in both closely resemble those produced by classic nonlinear baroclinic instabilities. In particular, the eddy momentum transport $u'v'$ generally converges on all the midlatitude jet cores while the eddy heat transport $v'T'$ peaks near the lower thermal interface and continuously relays the heat poleward across and between the multiple jets. In the chosen parameter range, four to five westerly jets normally form but none occur closer to the equator than 17°S unless an additional source of baroclinicity is introduced in lower latitudes; otherwise, an easterly current normally forms in the Tropics and at the equator. When a stronger baroclinicity does exist in low latitudes, the resulting W_1 jet can develop a barotropic instability that generates waves that slowly drive a westerly current at the equator, a current that equilibrates by gradually eliminating the eddy source. The W_1 jet and its instabilities do not, however, produce an equatorial westerly if they are centered much farther from the equator than the critical latitude at 8°S for Jovian parameters and at 25°S for terrestrial parameters.

Although they migrate, jets in the EXP system also exhibit the classic eddy characteristics associated with nonlinear baroclinic instabilities but with all fluxes confined to an upper layer that is close to having a neutral static stability. The eddy momentum transport $u'v'$ is confined to a particularly shallow upper surface layer while the eddy heat transport $v'T'$ is limited more to zones between the jets than in the LIN system and provides a discontinuous poleward transfer. Asymmetries in the converging $u'v'$ flux within each jet core, as well as the peaking of the $v'T'$ and Eliassen–Palm fluxes between the jets, may be the cause of the migration and may be attributable to the character of the baroclinic instability and wave dispersion in the EXP system. The standard diagnostics are not really suitable for defining the migration dynamics as the process is so weak.

Again, four or five jets form in the EXP system under the elementary $P_2(\phi)$ heating distribution but the W_1 jet now lies in lower latitudes, at 12°S , than its LIN counterpart. However, the system still requires that the baroclinicity be extended into lower latitudes to give a W_1 jet near enough to the equator for its barotropic instability to generate a W_0 current; but, unlike the LIN case, the baroclinicity does not need to be stronger in low latitudes than in midlatitudes to do this. Nevertheless, the resulting W_1 instability is significantly stronger in the EXP system than the LIN, and this results in a blending of the W_0 and W_1 currents into a broad flow that blocks other jets migrating from higher latitudes at 20°S ,

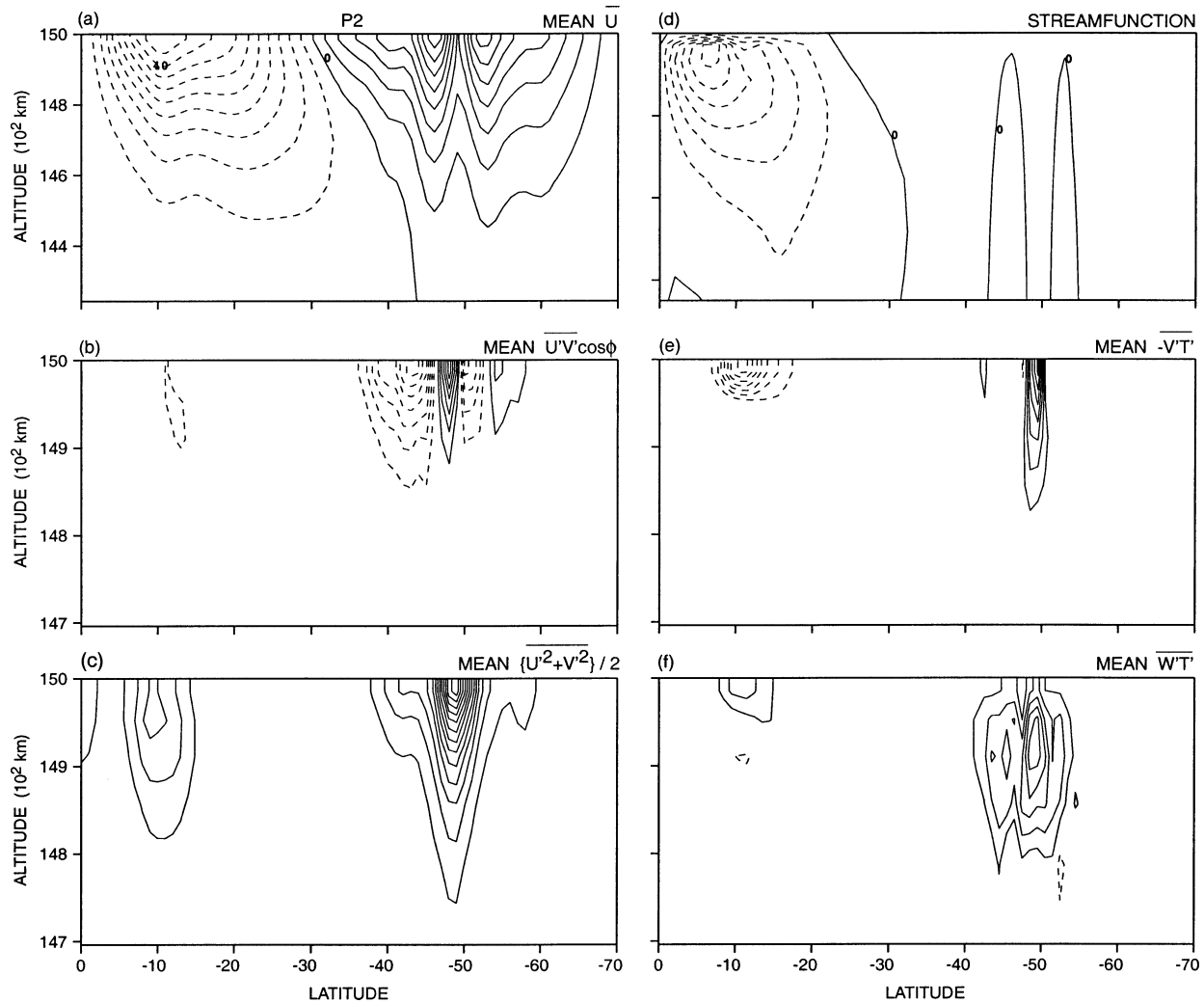


FIG. 21. Meridional sections of the primary fields and eddy transports for the P2 solution for a variable depth layer. The means are based on daily averages over 500–1000 days. In order, the contour interval, maximum, and minimum values are (a) (5, 43, -49) m s^{-1} , (b) (1, 6.6, -7.3) $\text{m}^2 \text{s}^{-2}$, (c) (5, 68, 0) $\text{m}^2 \text{s}^{-2}$, (d) (5, 4.7, -32) $\times 10^2 \text{m}^2 \text{s}^{-1}$, (e) (2, 14.7, -14.4) $\times 10^{-2} \text{C m s}^{-1}$, and (f) (5, 27.4, -7.8) $\times 10^{-5} \text{C m s}^{-1}$. The zero-value contours are omitted for the eddy fields.

a latitude where the W_2 and W_3 jets proceed to merge every 5000 days. To prevent westerlies from occurring at the equator, the heating has to produce a barotropic zone between the equator and 9°S that allows an easterly to form therein that is strong enough to stop the jets from displacing it.

The nature of the low-latitude instability is more clearly apparent when the W_1 jet exists alone in either the thin Jovian or thick terrestrial system. For Earth, the type of instability appears to depend primarily on the location of the baroclinic zone, for the novel form mainly occurs when the flow is driven by a baroclinicity that lies in lower latitudes than usual; otherwise, a classic jet and instability occur; see Williams (2003a) for further details. For midlatitude jets, the eddy momentum flux $u'v'$ is usually poleward but this switches sign to become mostly equatorward when the baroclinic zone

is moved to lower latitudes. In the limit, this flux can lead to an equatorial superrotation and maintain a jet at 20°S rather than at the usual 40°S location of the standard case. Such a circulation could exist on a planet with a glacial climate.

Although both structural systems fail to produce any real easterly jets (except at the equator), such flows can be generated quite easily, even for the elementary $P_2(\phi)$ source of heat, by allowing the heat to penetrate to (or originate at) depths that increase monotonically with latitude. A factor of 2 in depth between the equator and 45°S suffices to reverse the baroclinicity in lower latitudes and split the hemispheric flow into broad easterly and westerly currents; these currents can also be modified by small-scale baroclinic instabilities that generate minijets within them.

Theoretically, the dynamics of the multiple jets in thin

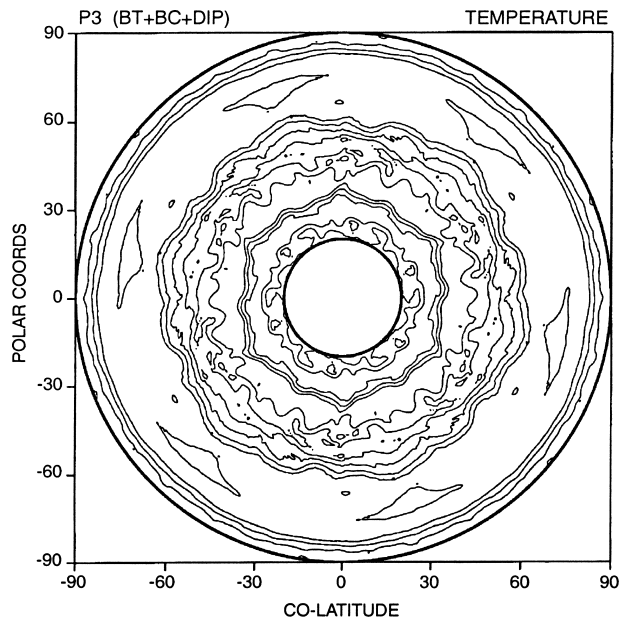


FIG. 22. Horizontal polar projection of the temperature field for the P3 solution at 500 days, sampled at a depth of 112 km. The contour interval, maximum, and minimum values are (0.4, 6.1, 0.2) °C, respectively.

systems is not well understood, particularly as regards the nonlinear processes that determine the jet scales. Given the weakness of the barotropic component, the Rhines β turbulence mechanism remains relevant only if viewed from the Held–Larichev perspective. Neither are the standard midlatitude and novel low-latitude forms of baroclinic instability understood for multiple jets in thin or thick layers, especially for the nonlinear phases that affect the jet formation and maintenance.

Turning to the planets, the solutions have some bearing on attempts to define the three-dimensional character of the flows on Jupiter and Saturn, within the limits set by the Boussinesq assumption. In particular, they indicate that multiple jets with realistic features can be generated from a *global-scale* heating that is confined to a thin vertical layer, a structure that also favors vortex formation (Part I). An extra baroclinicity component in low latitudes, however, helps make the flows more realistic in the Tropics and at the equator; either latent heating or albedo variations could provide such a component. However, the absence of the baroclinic easterly jets needed to generate large vortices such as the Great Red Spot suggests that once the $P_2(\phi)$ heating has created the westerly jets, the flow needs to produce stronger easterlies by activating, possibly through the albedo or latent heating, a sinusoidal $P_{10}(\phi) \sim \cos(5\phi)$ heating mode commensurate with the scale of the five jets.

To do this we envision a heating profile of the form $P(\phi) = \{P_2[1 - \mathcal{A}(t)] + P_{10}\mathcal{A}(t)\}$, where \mathcal{A} represents a growing albedo or latent heat related factor of the form $\mathcal{A}(t) = [1 - \exp(-(t/t_0)^4)]$, and t_0 is a timescale long enough to let the original jets form and set the

latitudinal scale before the jet-dependent albedo or latent heat variations become influential. The possibility of albedo-controlled circulations is noted by Green (1999, section 12.7). However, the scarcity of vortices in Jupiter's Northern Hemisphere undermines the need for such a complete $P_2 \rightarrow P_{10}$ transition in the heating. Elsewhere, the hexagonal jet seen on Saturn could indicate the presence of a nonlinear baroclinic instability in a thin dynamical layer; while the easterly current on Neptune could be due to the heated layer becoming thicker with increasing latitude.

So is the baroclinic thin-layer hypothesis adequate for theorizing about the Jovian atmospheres or does it need modification? So far, the hypothesis has mainly been studied using a variety of standard dynamical models so the conditions under which it gives relevant solutions are well defined. But the need for baroclinic easterlies implies that physical processes must be included and these may introduce ambiguities. However, other representations of the thin layer, other parameter ranges, or other heat sources may be less constrained. On the other hand, the limitations may be real and indicative of a need to extend or even replace the basic hypothesis. There may be many ways of producing multiple jets. Clearly, we have barely begun to approach the subtleties of the Jovian system.

Acknowledgments. Special thanks go to Catherine Raphael for organizing the graphics. I am also greatly indebted to Robert Hallberg, Isaac Held, Conway Leovy, and the reviewers for perceptive comments that helped improve this presentation, while discussions with Shafer Smith improved its content.

REFERENCES

- Allison, M., 2000: A similarity model for the windy Jovian thermocline. *Planet. Space Sci.*, **48**, 753–774.
- , D. A. Godfrey, and R. F. Beebe, 1990: A wave dynamical interpretation of Saturn's polar hexagon. *Science*, **247**, 1061–1063.
- Andrews, D. G., and M. E. McIntyre, 1978: Generalized Eliassen–Palm and Charney–Drazin theorems for waves on axisymmetric mean flows in compressible atmospheres. *J. Atmos. Sci.*, **35**, 175–185.
- Atkinson, D. H., J. B. Pollack, and A. Seiff, 1998: The *Galileo* Probe Doppler Wind Experiment: Measurement of the deep zonal winds on Jupiter. *J. Geophys. Res.*, **103** (E10), 22 911–22 928.
- Benilov, E. S., 1995: Baroclinic instability of quasi-geostrophic flows localized in a thin layer. *J. Fluid Mech.*, **288**, 175–199.
- Busse, F. H., 1994: Convection driven zonal flows and vortices in the major planets. *Chaos*, **4**, 123–134.
- Cho, J. Y.-K., and L. M. Polvani, 1996: The emergence of jets and vortices in freely evolving, shallow-water turbulence on a sphere. *Phys. Fluids*, **8**, 1531–1552.
- Condie, S. A., and P. B. Rhines, 1994: A convective model for the zonal jets in the atmospheres of Jupiter and Saturn. *Nature*, **367**, 711–713.
- Edmon, H. J., B. J. Hoskins, and M. E. McIntyre, 1980: Eliassen–Palm cross sections for the troposphere. *J. Atmos. Sci.*, **37**, 2600–2616.
- Feldstein, S. B., 1991: A comparison of the weakly nonlinear insta-

- bility of westerly and easterly jets in a two-layer beta-plane model. *J. Atmos. Sci.*, **48**, 1701–1717.
- Fjortoft, R., 1951: Stability properties of large-scale atmospheric disturbances. *Compendium of Meteorology*, T. F. Malone, Ed., Amer. Meteor. Soc., 454–462.
- Gierasch, P. J., 1976: Jovian meteorology: Large scale moist convection. *Icarus*, **29**, 445–454.
- Gill, A. E., 1982: *Atmosphere–Ocean Dynamics*. Academic Press, 662 pp.
- , J. S. A. Green, and A. J. Simmons, 1974: Energy partition in the large-scale ocean circulation and the production of mid-ocean eddies. *Deep-Sea Res.*, **21**, 499–528.
- Green, J., 1999: *Atmospheric Dynamics*. Cambridge University Press, 213 pp.
- Held, I. M., and A. Y. Hou, 1980: Nonlinear axially symmetric circulations in a nearly inviscid atmosphere. *J. Atmos. Sci.*, **37**, 515–533.
- , and V. D. Larichev, 1996: A scaling theory for horizontally homogeneous, baroclinically unstable flow on a beta plane. *J. Atmos. Sci.*, **53**, 946–952.
- Huang, H.-P., and W. A. Robinson, 1998: Two-dimensional turbulence and persistent zonal jets in a global barotropic model. *J. Atmos. Sci.*, **55**, 611–632.
- , B. Galperin, and S. Sukoriansky, 2001: Anisotropic spectra in two dimensional turbulence on the surface of a rotating sphere. *Phys. Fluids*, **13**, 225–240.
- Ingersoll, A. P., P. J. Gierasch, D. Banfield, and A. R. Vasavada, 2000: Moist convection as an energy source for the large scale motions in Jupiter's atmosphere. *Nature*, **403**, 630–632.
- Killworth, P. D., 1980: Barotropic and baroclinic instability in rotating stratified fluids. *Dyn. Atmos. Oceans*, **4**, 143–184.
- Lee, S., 1997: Maintenance of multiple jets in a baroclinic flow. *J. Atmos. Sci.*, **54**, 1726–1738.
- Limaye, S. S., and L. A. Sromovsky, 1991: Winds of Neptune: *Voyager* observations of cloud motions. *J. Geophys. Res.*, **96**, 18 941–18 960.
- Orsolini, Y., and C. B. Leovy, 1993: A model of large scale instabilities in the Jovian troposphere. 1. Linear model. *Icarus*, **106**, 392–405.
- Panetta, R. L., 1993: Zonal jets in wide baroclinically unstable regions: Persistence and scale selection. *J. Atmos. Sci.*, **50**, 2073–2106.
- Rhines, P. B., 1975: Waves and turbulence on a beta plane. *J. Fluid Mech.*, **69**, 417–443.
- , 1977: The dynamics of unsteady currents. *The Sea*, E. D. Goldberg et al., Eds., *Marine Modeling*, Vol. 6, Wiley and Sons, 189–318.
- , 1994: Jets. *Chaos*, **4**, 313–339.
- Salmon, R., 1998: *Lectures in Geophysical Fluid Dynamics*. Oxford University Press, 378 pp.
- Saravanan, R., 1993: Equatorial superrotation and maintenance of the general circulation in two-level models. *J. Atmos. Sci.*, **50**, 1211–1227.
- Seiff, A., and Coauthors, 1998: Thermal structure of Jupiter's atmosphere near the edge of a 5- μm hot spot in the north equatorial belt. *J. Geophys. Res.*, **103** (E10), 22 857–22 889.
- Simmons, A. J., and B. J. Hoskins, 1978: The life cycles of some nonlinear baroclinic waves. *J. Atmos. Sci.*, **35**, 414–432.
- Simon, A. A., 1999: The structure and temporal stability of Jupiter's zonal winds: A study of the north tropical region. *Icarus*, **141**, 29–39.
- Smagorinsky, J., 1963: General circulation experiments with the primitive equations. 1. The basic experiment. *Mon. Wea. Rev.*, **91**, 99–164.
- Smith, K. S., and G. K. Vallis, 2002: The scales and equilibration of midocean eddies: Forced-dissipative flow. *J. Phys. Oceanogr.*, **32**, 1699–1720.
- Spar, J., 1957: A note on the stability of baroclinic waves. *J. Meteor.*, **14**, 136–140.
- Suarez, M. J., and D. G. Duffy, 1992: Terrestrial superrotation: A bifurcation of the general circulation. *J. Atmos. Sci.*, **49**, 1541–1554.
- Treguier, A. M., and R. L. Panetta, 1994: Multiple zonal jets in a quasigeostrophic model of the Antarctic circumpolar current. *J. Phys. Oceanogr.*, **24**, 2263–2277.
- Vallis, G. K., and M. E. Maltrud, 1993: Generation of mean flows and jets on a beta plane and over topography. *J. Phys. Oceanogr.*, **23**, 1346–1362.
- Wiin-Nielsen, A., 1967: On baroclinic instability as a function of the vertical profile of the zonal wind. *Mon. Wea. Rev.*, **95**, 733–739.
- Williams, G. P., 1978: Planetary circulations: 1. Barotropic representation of Jovian and terrestrial turbulence. *J. Atmos. Sci.*, **35**, 1399–1426.
- , 1979: Planetary circulations: 2. The Jovian quasi-geostrophic regime. *J. Atmos. Sci.*, **36**, 932–968.
- , 1988: The dynamical range of global circulations—I. *Climate Dyn.*, **2**, 205–260.
- , 1996: Jovian dynamics. Part I: Vortex stability, structure, and genesis. *J. Atmos. Sci.*, **53**, 2685–2734.
- , 1997: Planetary vortices and Jupiter's vertical structure. *J. Geophys. Res.*, **102** (E4), 9303–9308.
- , 2002: Jovian dynamics. Part II: The genesis and equilibration of vortex sets. *J. Atmos. Sci.*, **59**, 1356–1370.
- , 2003a: Baroclinic instability and equatorial superrotation. *J. Atmos. Sci.*, in press.
- , 2003b: Jet sets. *J. Meteor. Soc. Japan*, in press.
- , and J. B. Robinson, 1973: Dynamics of a convectively unstable atmosphere: Jupiter? *J. Atmos. Sci.*, **30**, 684–717.
- , and R. J. Wilson, 1988: The stability and genesis of Rossby vortices. *J. Atmos. Sci.*, **45**, 207–241.
- Young, R. E., 1998: The *Galileo* probe mission to Jupiter: Science review. *J. Geophys. Res.*, **103** (E10), 22 775–22 790.